https://dx.doi.org/10.1016/j.engstruct.2019.109494

Structural behaviour and design of high strength steel RHS X-joints

Xiaoyi Lan[a], Tak-Ming Chan[a,*], Ben Young[a,1]

[a] Dept. of Civil and Environmental Engineering, The Hong Kong Polytechnic University, Hong Kong, China
[1] Formerly, Dept. of Civil Engineering, The University of Hong Kong, Pokfulam Road, Hong Kong, China
*tak-ming.chan@polyu.edu.hk

Abstract: This paper aims to investigate the structural behaviour and static strength of high strength steel rectangular hollow section (RHS) X-joints under axial compression in the braces through tests and numerical analysis. Eight RHS X-joints which were composed of fabricated steel tubes with a measured yield stress of 907 MPa were tested. Extensive numerical simulations on the fabricated RHS X-joints in S460, S690 and S960 steel were conducted using finite element (FE) analysis. The FE model was validated against the test results. The investigated failure modes are chord face plastification, chord side wall failure and a combination of these two failure modes. The effects of the heat affected zones (HAZ) and suitability of the strength equations adopted by the CIDECT design guide for the fabricated RHS X-joints were examined. The deformation capacity and ductility of test specimens which failed by chord face plastification could be considered as reasonably sufficient. The effects of material strength reduction in the HAZ on the joint initial stiffness are minor, but could significantly lower the joint strength. In general, the CIDECT strength prediction is increasingly unconservative with increasing steel grade for the RHS X-joints failing by chord face plastification. However, the CIDECT strength prediction is generally conservative for the combined failure modes, and becomes increasingly conservative with increasing chord side wall slenderness for chord side wall failure. The suggested ranges of brace to chord width ratio (β) and chord width to wall thickness ratio (2γ) are $0.4\leq\beta\leq0.85$ and $2\gamma\leq60\beta-1$ for the RHS X-joints failing by chord face plastification to allow for more effective use of high strength steel, and corresponding strength equations were proposed. An analytical model of plate buckling was proposed and the deformation-based continuous strength method (CSM) originally developed for designing non-slender stainless steel cross-sections was adopted for the design of chord side wall failure in the RHS X-joints with β=1.0 and 2γ up to 50. The proposed design method is also applicable for designing chord side wall failure in equal-width RHS X-joints using cold-formed and hot-finished carbon steel and cold-formed stainless steel. A linear interpolation approach using the proposed strength equations at β=0.85 and β=1.0 is suggested for the RHS X-joints with $0.85<\beta<1.0$ and $2\gamma\leq50$ which failed by the combined failure modes. The proposed strength equations can produce much more accurate and consistent strength prediction than the CIDECT design guide, and were converted to design strength equations for the design of high strength steel RHS X-joints.

Keywords: High strength steel; RHS X-joint; Structural behaviour; Structural design; Static strength

1. Introduction

Advances of steel production techniques such as quenching and tempering (QT) and thermo-mechanical controlled processing (TMCP) have led to readily available high strength steel (HSS) with acceptable ductility and toughness nowadays [1]. HSS with nominal yield stresses higher than 450 MPa is increasingly popular in the infrastructure sector as an economic and sustainable construction material. The application of HSS with high strength-to-weight ratio in onshore and offshore tubular structures could lower construction costs because of reduced member sizes and structural self-weights. Less consumption of energy and resources for HSS tubular structures due to material savings could also contribute to reduced carbon footprints. Design guidance for HSS tubular joints which are vitally critical components for the structural integrity is imperatively needed to facilitate structural applications of HSS tubular structures.

Design rules for tubular joints which are composed of hot-finished or cold-formed normal strength steel tubes are specified in design codes and guides e.g. Eurocode EN 1993-1-8 [2] and the CIDECT design guides [3, 4]. EN 1993-1-8 [2] allows for the use of steel grades greater than S355, but stipulates a reduction factor of joint strength of 0.9 for tubular joints in steel grades greater than S355 and up to S460. EN 1993-1-12 [5] further extends the material limitation to S700 and imposes a reduction factor of 0.8 for steel grades higher than S460 and up to S700. Likewise, the CIDECT design guides [3, 4] also require the application of a reduction factor of 0.9 combined with the limitation of the yield strength (f_y) to 0.8 times the ultimate strength (f_u). The restrictive design rules for steel grades beyond S355 are primarily based on the findings reported by Liu and Wardenier [6] and Kurobane [7] that the static strengths of RHS and CHS gap K-joints in S460 steel are lower than those of S235 joints in relative terms. However, the suitability of such design rules for all HSS tubular joints regardless of failure modes remains controversial. Experimental and numerical investigations have been carried out to re-evaluate the design rules for HSS tubular joints in recent years.

Recent research on HSS circular hollow section (CHS) joints has been mostly focused on CHS X-joints. Tests and numerical simulations on CHS X-joints in steel grades ranging from S460 to S770 and under axial compression, tension or in-plane bending in the braces have been conducted by Puthli et al. [8] and Lee et al. [9]. The failure modes examined are chord face plastification and chord punching shear. It is found that the test and numerical joint strengths are generally higher than the design strengths predicted by the EN 1993-1-8 [2] without applying the reduction factors, and the test specimens have sufficient deformation capacity and ductility. Lan et al. [10, 11] conducted extensive numerical simulations on CHS X-joints using steel grades varying from S460 to S1100 and subjected to axial compression in the braces which failed by chord face plastification. It is found that the effects of the heat affected zones on the initial stiffness and static strength of the X-joints could be insignificant, and the CIDECT mean strength prediction is increasingly unconservative with increasing steel grade. Design rules which allow for reasonably effective use of HSS were proposed for the X-joints.

Structural performance of HSS rectangular hollow section (RHS) joints has also been re-assessed. Becque and Wilkinson [12] conducted tests on T- and X-joints using C450 steel with a nominal yield stress of 450 MPa and subjected to axial compression or tension in the braces. It is found that the test joint strengths are higher than the CIDECT nominal strengths without using the reduction factor and limitation on the yield stress for chord face plastification and chord side wall failure. However, the test strengths are lower than the CIDECT nominal strengths for chord punching shear and effective width failure of braces justifying the application of the reduction factor and limitation on yield stress. Mohan et al. [13] carried out numerical simulations on axially loaded RHS K- and N-joints in C450 steel. The numerical joint strengths exceed the CIDECT design strengths without using the reduction factor and limitation on yield stress. Havula et al. [14] conducted tests on square hollow section (SHS) T-joints using S420, S500 and S700 steel and subjected to in-plane bending in the braces which failed by chord face plastification. It is found that the test moment resistances of T-joints using large fillet welds, and the S420 and S500 steel T-joints using small fillet welds exceed the Eurocode design strengths without using the reduction factors except for the butt-welded T-joints and the S700 steel T-joints with small fillet welds. Deformation capacity and ductility of the test specimens are sufficient. Feldmann et al. [15] assessed the suitability of the reduction factors against test results of RHS X- and K-joints in S500, S700 and S960 steel which failed by chord face plastification, chord side wall failure, chord punching shear, chord shear and weld failure. The test ultimate loads without considering deformation limits generally exceed the Eurocode design strengths using the reduction factors. The static strengths of RHS X-joints in S960 steel and subjected to axial compression in the braces have also been experimentally investigated by Pandey and Young [16]. It is found that the Eurocode and CIDECT design strength predictions without using the reduction factors are unconservative for the RHS X-joints failing by chord face plastification and become conservative for chord side wall failure and a combination of chord face plastification and chord side wall failure. A comprehensive review on the recent research advances of HSS hollow section joints under static and fatigue loadings was summarised in Lan and Chan [1].

The aforementioned investigations have been focused on cold-formed or hot-finished HSS tubular joints which are commonly used in light-weight tubular structures. Tubular joints which are composed of fabricated steel tubes are generally preferred in the case of heavy loading. However, research on the structural behaviour and static strength of HSS fabricated tubular joints remains limited, and corresponding design rules are needed. This project examined the structural performance of fabricated RHS X-joints in steel grades ranging from S460 to S960 and subjected to axial compression in the braces. Tests were conducted on eight fabricated RHS X-joints with a measured yield stress of 907 MPa. The chord face indentation and chord sidewall deformation of the test specimens were measured. A finite element (FE) model was developed and validated against the obtained test results. Upon verification of the FE model, extensive numerical simulations were conducted to examine the effects of heat affected zones (HAZ) and suitability of current CIDECT design provisions for HSS RHS X-joints. Design rules allowing for reasonably effective use of HSS are proposed for the X-joints in this study.

2. Experimental investigation

2.1. Test specimens

Eight fabricated RHS X-joint specimens which were composed of fabricated steel tubes were tested under axial compression in the braces. The steel tubes were fabricated from four steel plates using full penetration butt welds at the tube corner and thereafter assembled into the RHS X-joint specimens by fillet welds at the brace-chord intersection as shown in Fig. 1. For the chord members, nominal overall flange width (b_0) and nominal overall web depth (h_0) range from 120 to 300 mm. The nominal overall flange width (b_1) and nominal overall web depth (h_1) of the braces vary from 60 to 150 mm. Three key joint parameters were examined in tests by varying brace to chord width ratio (β) from 0.50 to 0.79, brace height to chord width ratio (η) from 0.50 to 0.81, and chord width to wall thickness ratio (2γ) from 19.8 to 49.1. The nominal chord length (L_0) was designed to be $6b_0$ to ensure that the stresses at the brace-chord intersection are not affected by the chord ends, and the nominal brace length (L_1) was taken as $3b_1$ to avoid the brace overall buckling [17]. The measured dimensions of test specimens are summarised in Table 1. All the steel tubes were fabricated from one parent steel plate with measured thickness of 6.14 mm, and thus the brace to chord wall thickness ratio (τ) is 1.0. The brace members were carefully positioned and then welded to the two chord faces at a right angle, and thus the angle between the brace and chord (θ) is 90°. The seam weld of chord members was positioned in the chord side walls as shown in Fig. 1, and end plates were welded to the brace ends to allow for uniform axial compression at the brace ends.

2.2. Material properties and welding

A Chinese Q890 high strength steel plate with a nominal yield stress of 890 MPa which was used for fabricating the steel tubes was manufactured by the Quenching and Tempering (QT) technique. The chemical compositions according to the mill certificate are listed in Table 2. The carbon equivalent value (CEV) of the steel plate is 0.56%. Two flat coupons (F1 and F2) with nominal gauge length of 50 mm, nominal gauge width of 12.5 mm and nominal thickness of 6 mm were machined from the steel plate. The letter (F) in the coupon labels (F1 and F2) denotes that the coupons were machined from the flat steel plate and the number (1 or 2) represents the coupon number. Fig. 2 shows the dimensions of coupons which conform the requirements of standard coupons specified in BS EN ISO 6892-1 [18] and ASTM E8/E8M specification [19]. A calibrated extensometer of 50 mm gauge length was used to measure the longitudinal strain of coupons during testing. Two linear TML strain gauges were attached to the centre of the gauge length on both surfaces of each coupon. The coupons were tested in an INSTRON hydraulic controlled testing machine with a loading rate of 0.1 mm/min up to around the 0.2% yield stress and 0.4 mm/min thereafter. Static engineering stress-strain curves eliminating the strain rate effect incorporated in the dynamic engineering stress-strain curves obtained from tests are shown in Fig. 3 which were obtained by pausing the applied displacement near the 0.2% yield stress, ultimate stresses and post-ultimate region for 2 minutes. Table 3 shows the measured material properties including the elastic modulus (E), static stress at 0.01% plastic strain (f_p), static 0.2% yield stress (f_y), static ultimate stress (f_u), ultimate strain at static ultimate stress (ε_u) and fracture strain (ε_f).

Gas metal arc welding (GMAW) was used in fabricating the X-joint specimens. The full penetration butt weld was adopted for manufacturing steel tubes at the tube corner and the fillet weld was employed to assemble the brace and chord into the X-joint specimens. The welds were designed in accordance with AWS D1.1/D1.1M [20]. The measured dimensions of the reinforcement of butt welds in chord members (b_w and h_w, see Fig. 1) and the weld leg size of fillet welds (w) are summarised in Table 1. The filler material was a low alloy carbon steel wire with a diameter of 1.2 mm which conformed to class ER120S-G of the AWS A5.28M specification, and the typical values of f_y, f_u and ε_f of the filler wire are 930 MPa, 980 MPa and 19%, respectively [16]. A robotic arm was used to perform the welding in order to allow for consistent heat input during welding and achieve satisfactory welding quality. The current, voltage and welding speed during welding were 150A, 16V and 300 mm/min, and the estimated heat input is 0.38 kJ/mm in accordance with the SSAB Welding Handbook [21].

2.3. Test set-up and procedures

A servo-controlled hydraulic testing machine with maximum capacity of 1000 kN was used to apply axial compression through the brace end of X-joint specimens. The test set-up is shown in Fig. 4. A special ball bearing was employed which was attached to an adjustable top support. The ball bearing can self-adjust according to the flat profile of brace end plates, and thus a uniform axial compressive load can be applied to the brace. At the beginning, the ball bearing was unlocked and can rotate freely. The actuator ram of the testing machine was then moved up slowly to a preload around 4 kN by a load-controlled mode. The small preload was applied in order to allow the ball bearing to self-adjust according to the brace end plate and therefore eliminate any possible gaps between the brace end plate and ball bearing. The position of ball bearing was locked afterwards by using four vertical bolts to restrict any major and minor axis rotations for the rest of testing. Therefore, the ball bearing can be considered as fixed-end, and only a pure axial compressive force without any bending moments from the actuator ram was applied to the brace end.

Calibrated linear variable displacement transformers (LVDTs) were employed to measure the deformations in the brace-chord intersection region. The chord face indentation (u) at the crown position (see Fig. 1) on each side of the brace member was measured using the extension arms attached to the tips of the LVDTs (e.g. LVDT No. 1 as shown in Fig. 4). The chord face indentation at the chord crown was measured along brace axial direction and at 12 mm from the adjacent brace face for all the tests. The chord side wall deformation (v) was measured by two horizontal LVDTs with Poly Methyl Methacrylate (PMMA) plates connecting to their tips (e.g. LVDT No. 2 as shown in Fig. 4). The use of PMMA plates facilitates the capture of maximum chord side wall deformations without being affected by the overall vertical displacement of the chord member during testing. The applied displacement of the actuator ram was also recorded by the LVDT (i.e. LVDT No. 3 as shown in Fig. 4).

After preloading, the testing was carried out by driving the actuator ram under a displacement-controlled mode which allows the test to be continued in the post-ultimate range. A constant loading rate of 0.3 mm/min was adopted. The applied load of testing machine and readings of the displacement transducers were recorded by a data acquisition system at regular intervals. It should be noted that the tests were paused for 2 minutes near the ultimate load or after the load at the indentation limit of 3%b_0 in order to allow for the static drops and thereafter to obtain the static load-deformation curves.

2.4. Test results

The eight fabricated RHS X-joint specimens in tests failed by chord face plastification as shown in Fig. 5. Figs. 6-7 show the obtained static loads (N) plotted against the chord face indentation (u) and chord side wall deformation (v). The joint strengths obtained from the static load-indentation curves of test specimens are summarised in Table 4. It should be noted that the static strength (N_{Test}) of RHS X-joints in this study was determined as the ultimate load or the load at an indentation limit of 3%b_0 at the crown, whichever occurred earlier, in accordance with the CIDECT design guide [3]. Figs. 6-7 show that the chord face indentation and chord side deformation can generally reach at least two times of the indentation limit of 3%b_0 as tabulated in Table 4, and brittle failure was not observed at large deformations. The deformation capacity and ductility of the test specimens could therefore be considered as reasonably sufficient. It should also be noted that repeated tests were conducted for the specimens X1 and X3. The obtained load-deformation curves from the repeated tests generally coincide with those of specimens X1 and X3, and the corresponding joint strengths are in good agreement with differences of 1.1% and 0.3% demonstrating reliability of the test results.

3. Finite element analysis

3.1. Finite element model

The general purpose finite element (FE) software ABAQUS [22] was used to carry out numerical simulations on HSS RHS X-joints in this study. A FE model was developed by validating against the test results described in Section 2.4. The measured geometric dimensions summarised in Table 1 were used to model the test specimens. An 8-node linear solid element with reduced integration (C3D8R) was selected to model the brace and chord members, and the fillet welds at the brace-chord intersection were modelled by a 10-node quadratic tetrahedron solid element (C3D10). A 6-node linear wedge solid element (C3D6) was adopted to simulate the reinforcement of butt welds in the chord and that of the butt welds in the brace was not modelled because brace failure was not observed in tests and the brace was only subjected to pure axial compression. Two layers of the solid element (C3D8R) through the tube wall thickness of the brace and chord were adopted. A mesh convergence study was conducted to determine suitable mesh sizes. The mesh sizes ranging from 5 to 12 mm which depend on the cross-section sizes were employed for the brace, chord and butt welds, and a mesh size of 3 mm was adopted for the fillet welds. The change of the predicted joint strengths resulted from reducing the mesh sizes is within 2% of the corresponding test strengths.

The static stress-strain curves and average material properties obtained from the tensile coupon tests described in Section 2.2 were adopted for the modelling of test specimens. The true stress and logarithmic plastic strain converted from the obtained engineering stress and strain were incorporated into the FE model. The Poisson's ratio of steel materials in this study was taken as 0.3. The von-Mises yield criterion and isotropic strain hardening rules were employed. Boundary conditions in the FE model were set in accordance with the test set-up in Section 2.3. One brace end was fixed and all degrees of freedom at the other brace end were restrained except for the brace axial displacement. The degrees of freedom at the two chord ends were not restricted, and thus the chord ends were free to translate and rotate. The parameter (*NLGEOM) was adopted to take into account the effect of geometric nonlinearity in FE analysis. The axial compressive load in the braces was applied in increments of displacement by using the (*Static) method in ABAQUS.

A comparison between the FE and test results was made to validate the adopted FE model. Fig. 5 shows the comparison of the failure mode of chord face plastification. It is shown that the adopted FE model can replicate the failure mode observed in tests. Figs. 6-7 show that the load-deformation curves obtained from FE simulations and tests generally coincide with each other. The comparison of joint strengths was summarised in Table 4. The numerical strengths (N_{FE}) are, in general, slightly lower than the obtained test strengths (N_{Test}). The mean value of N_{FE}/N_{Test} ratio is 0.93 with corresponding coefficient of variation (COV) of 0.057. It is therefore demonstrated that the developed FE model can produce reasonably accurate prediction of the structural behaviour and static strength of fabricated RHS X-joints. The validated FE model will be adopted for the subsequent FE simulations. It should be noted that all test specimens failed by chord face plastification. The failure modes in this study are defined in line with the CIDECT design guide [3] i.e. chord face plastification for the RHS X-joints with $\beta \leq 0.85$, chord side wall failure for $\beta=1.0$ and the combined failure modes for $0.85<\beta<1.0$. These failure modes are mainly controlled by the chord face indentation or chord side wall deformation, whichever governs the structural responses and static strengths of the joints. It is noted that the chord side walls of test specimens also deformed significantly in tests (see Fig. 7). Figs. 6-7 show that the load-chord face indentation curves and load-chord side wall deformation curves predicted by the adopted FE models can agree well with those in tests. This demonstrates that the developed FE models can capture the structural behaviours and deformations of the RHS X-joints well, and therefore can also be used to predict other failure modes e.g. the chord side wall failure in which the chord side wall deformation typically dominates the X-joint responses.

3.2. Effects of heat affected zones

The microstructures and material properties of heat affected zones (HAZ) resulted from the heat input into base metals during welding could be different from those of base metals. The material properties of

HAZ mainly depend on the steel material (e.g. TMCP or QT steel), heat input, welding type (e.g. GMAW or laser welding) and cooling time [11]. Stroetmann et al. [23] found that the ultimate stresses (f_u) of HAZ in QT S690Q and S960Q steel as well as TMCP S500M steel are generally higher than those of base metals except for the TMCP S700M steel, possibly because of optimised micro-alloying in TMCP steel when compared with QT steel. Similar findings indicating that the strength reduction of direct quenching (DQ) S960 steel is around 20% while that of QT S960 steel is insignificant were reported by Siltanen et al. [24]. The results show that the strength reduction in HAZ of HSS could be larger for higher steel grades and more pronounced for TMCP and DQ HSS when compared with QT HSS. Low heat input could mitigate the strength reduction in HAZ or even lead to higher strengths in QT HSS while high heat input may result in significant strength reduction in HAZ of HSS [25]. The strength reduction in the HAZ could be significant for HSS if welding parameters are not properly controlled. It is therefore imperative to provide suitable welding guidance for HSS, and related research is urgently needed.

It is necessary to investigate the effects of HAZ on the stiffness and static strength of the fabricated RHS X-joints because the strength reduction of HAZ in HSS could occur in practice. FE simulations were conducted on the RHS X-joints in ultra-high steel grade of S960 as summarised in Table 5 because the strength reduction of HAZ for lower steel grades is relatively minor [23, 25]. The measured dimensions of specimens X1, X3 and X6 in tests were adopted for numerical simulations. The geometric parameters of specimens X1-1, X1-2 and X1-3 are the same as those of specimen X1, except for the brace width and height or wall thickness of the brace and chord, and the dimensions of specimen X3-1 are identical to those of specimen X3 except for the brace width and height. The developed FE model in Section 3.1 were adopted to carry out the numerical analysis. Fig. 8 shows the HAZ in the analysed RHS X-joints using S960 steel. The sizes and material properties of HAZ were determined in accordance with Lan et al. [11], which are based on the test results of HAZ reported by Siltanen et al. [24] and Javidan et al. [25]. The width of HAZ resulted from the heat input of fillet welds equals to t_1+w+12 mm. The widths of HAZ due to the chord butt welds at the tube corner were conservatively taken as t_0 in the chord faces and 15 mm for the chord side walls considering the profile of butt welds (see Fig. 1). The notations of t_0 and t_1 refer to the chord and brace wall thickness, respectively, and w is the fillet weld leg size. The HAZ was assumed to cover the full tube wall thickness because of the relatively thin walls of the chord member. It should be noted that the HAZ in the braces was not modelled because brace cross-section capacity was higher than the static strength of analysed joints and brace failure did not occur. The reduction of yield stress (f_y) and ultimate stress (f_u) in HAZ adjacent to the fillet welds and butt welds which is in red colour as shown in Fig. 8 was taken as 20% and the strength reduction of HAZ far from the welds which is in blue (see Fig. 8) equals to 10%. The ultimate strain at ultimate stress (ε_u) of HAZ near the welds (in red) was taken as 2.1 times of the ultimate strain of the base metal of S960 steel [25], and the elastic modulus (E) of HAZ was taken as that of the base metal. The material properties of base metal of S960 steel in Ban and Shi [26] and those of HAZ adopted herein are summarised in Table 6. The corresponding engineering stress-strain curves adopted for the base metal and HAZ which were obtained from the multi-linear stress-strain curve model proposed by Ban and Shi [26] are shown in Fig. 9 (b).

Fig. 10 shows the load-indentation curves of the S960 steel RHS X-joints without and with HAZ obtained from FE analysis. It is shown that the effect of HAZ on the initial stiffness of the X-joints investigated is insignificant. This is because the initial joint stiffness mainly depends on joint geometric parameters and steel elastic modulus. However, the HAZ could lower the stiffness and static strength of the X-joints when plastic deformation occurred at the brace-chord intersection due to the material strength reduction in HAZ. Table 5 summarises the static strengths of analysed RHS X-joints without HAZ (N_{u1})

and with HAZ (N_{u2}). It is shown that the reduction of static strength varies from 1 to 8% for the RHS X-joints analysed with small or large β ratio (i.e. β=0.20, 0.79 and 1.00) and 2γ ratio ranging from 10.0 to 50.0. However, the joint strength reduction is up to 15% for the RHS X-joints with medium β ratio (i.e. β=0.50) and 2γ ratio ranging from 20.0 to 49.1. This is because the failure mode for the RHS X-joints with large β ratio is chord side wall failure or a combination of chord face plastification and chord side wall failure which mainly depends on the cross-section yielding or plate buckling of the chord side walls. The effect of strength reduction of HAZ which is in the chord faces and at the tube corners (see Fig. 8) could therefore be minor on the chord side wall failure which typically occurs in the middle of chord side walls. However, the strength reduction of RHS X-joints with medium β ratio which failed by chord face plastification is more pronounced. The chord face plastification typically involves the formation of yield lines in the chord faces at the brace-chord intersection. The strength reduction of HAZ in the chord faces could therefore lower the joint strength more significantly. It is noted that the strength reduction of RHS X-joints with small β ratio (i.e. β=0.20) which failed by chord face plastification is less significant when compared with that in the X-joints with medium β ratio (i.e. β=0.50). This is because the increased yield stress of high strength steel is increasingly under-utilised with decreasing β ratio in the RHS X-joints failing by chord face plastification, and the stresses in the joints are mostly elastic which will be discussed in Section 4.2.2. This therefore mitigates the strength reduction of the RHS X-joints with small β ratio resulted from the material strength reduction in the HAZ. In addition, the membrane action develops when the chord faces bend resulting in tensile chord axial stresses which can resist the compressive brace loading. The membrane effect in the chord faces of the RHS X-joints with smaller β ratio is more significant.

The reduction of joint strength is less pronounced than the material strength reduction adopted. This could be attributed to the redistribution of plastic stresses in HAZ to nearby base metals and the under-utilisation of the improved yield stresses of HSS in the RHS X-joints failing by chord face plastification which will be discussed in Section 4.2.2. It is also noteworthy that the material strength reduction and sizes of HAZ adopted in the FE simulations for the S960 RHS X-joints are relatively large and could be smaller if optimised welding parameters are employed which could lead to minor joint strength reduction. Furthermore, the joint strength reduction could be less significant for the RHS X-joints using QT HSS than that of the X-joints in TMCP or DQ HSS because of less pronounced material strength reduction in HAZ of QT HSS [23-25]. The HAZ was therefore not explicitly modelled in the parametric FE analysis described in Section 3.3. However, the joint strength reduction resulted from the HAZ was considered by proposing conservative strength equations for the HSS RHS X-joints which will be discussed in Section 5.

3.3. Parametric study

A parametric study on a total of 585 RHS X-joints in S460, S690 and S960 steel was conducted. For each steel grade, 195 RHS X-joints were analysed including 99 specimens without chord preload and 96 specimens subjected to chord preload. For the RHS X-joints without chord preload, 11 series of specimens were analysed as shown in Table 7, by varying the ratio (β) of brace width (b_1) to chord width (b_0) from 0.3 to 1.0, the ratio (η) of brace height (h_1) to chord width (b_0) from 0.3 to 2.0, and aspect ratio (ζ) of chord height (h_0) to chord width (b_0) from 0.5 to 2.0. For each series, 9 values of wall thickness (i.e. 9.6, 10.7, 12, 13.7, 16, 19.2, 24, 32 and 48 mm) were employed for the brace and chord members and the ratio (2γ) of chord width (b_0) to chord wall thickness (t_0) varied from 10 to 50. The ratio (τ) of brace wall thickness (t_1)

to chord wall thickness (t_0) and the angle between the brace and chord (θ) were set to be 1.0 and 90°, respectively. Among the 11 series of specimens without chord preload, 12 X-joint configurations with $\beta=\eta=0.3$, 0.5, 0.8, 1.0 and $2\gamma=10$, 25, 40 were selected to examine effects of chord preload ratio (n) which is the ratio of the chord preload (N_p) to the chord cross-section yield load (Af_y). Eight values of chord preload ratio of -0.8, -0.6, -0.4, -0.2, 0.2, 0.4, 0.6 and 0.8 were investigated, and the negative and positive values refer to compression and tension, respectively. The length of chord members (L_0) was set to be $6b_0$ and the brace length (L_1) was taken as b_1+h_1. The welds at the brace-chord intersection on the chord faces were modelled in accordance with the minimum requirements for butt welds specified in AWS D1.1/D1.1M [20], and the reinforcement of the chord butt welds was not modelled, in order to provide lower bound strength prediction for the RHS X-joints in practice. The investigated parameter ranges herein are $0.3\leq\beta\leq1.0$, $0.3\leq\eta\leq2.0$, $0.5\leq\zeta\leq2.0$, $10\leq2\gamma\leq50$ and $-0.8\leq n\leq0.8$.

The material properties tabulated in Table 6 and engineering stress-strain curve models (see Fig. 9) of S460, S690 and S960 steel proposed by Ban and Shi [26] were adopted for the parametric study. The FE model developed in Section 3.1 were employed. Four layers of the solid element (C3D8R) through the tube wall thickness of the brace and chord were adopted for the X-joints with $2\gamma<20$ while two layers of the solid element was employed for the X-joints with $2\gamma\geq20$. A mesh convergence study was conducted and it is found that mesh sizes of 20 mm for the brace and chord members and $t_1/6$ for the fillet welds are suitable. For the RHS X-joints without chord preload, the two chord ends were free to translate and rotate and all degrees of freedom at the two brace ends were restricted except for the brace axial displacement. The axial compression in the braces was applied by means of displacement. For the RHS X-joints with chord preload, all degrees of freedom at the brace and chord ends were restrained except for the axial displacement. The chord preload was applied to the chord and thereafter the brace ends were loaded by displacement. It should be noted that brace failure occurred in the analysed S460, S690 and S960 steel specimens with $b_0=b_1=240$ mm, $h_0=h_1=480$ mm, $t_0=t_1=48$ mm and without chord preload. Local buckling of the chord member occurred in some specimens with $2\gamma=40$ and subjected to large chord preload. Those specimens are joints with $\beta=0.3$, 0.5, 0.8 and $n=-0.8$ for S460 steel, $\beta=0.3$, 0.5, 0.8, 1.0 and $n=-0.8$ for S690 steel, and $\beta=0.3$, 0.5, 0.8, 1.0 and $n=-0.6$, -0.8 for S960 steel. The FE results of these specimens which failed by brace or chord member failure will be excluded in the subsequent analysis.

4. Evaluation of design rules for HSS RHS X-joints

4.1. Current design rules for RHS X-joints

Design rules for hot-finished and cold-formed normal strength steel RHS X-joints are stipulated in design codes and guides e.g. EN 1993-1-8 [2] and the CIDECT design guide [3]. It is noted that the design provisions specified in EN 1993-1-8 [2] for the RHS X-joints are in line with those in the 2nd edition of IIW recommendations [27], which prescribes no reduction of joint strengths for tensile chord axial stresses and takes the ultimate loads as the joint strengths. The 3rd edition of IIW recommendations [28] on which the 2nd edition of the CIDECT design guide [3] is based updates the chord stress equation (Q_f) to quantify the detrimental effects of tensile and compressive chord axial stresses on the joint strength more accurately and adopts the indentation limit of $3\%b_0$. The background of the revised design rules for tubular joints adopted by the 3rd edition of IIW recommendations [28] is elaborated in Wardenier et al. [29]. The design rules for the RHS X-joints in the CIDECT design guide [3] are therefore evaluated in the following subsection.

The CIDECT design strength equations for the RHS X-joints with $\beta \leq 0.85$ and under axial compression in the braces which failed by chord face plastification are as follows:

$$N_{\mathrm{CIDECT,Rd}} = Q_{\mathrm{u}} Q_{\mathrm{f,CIDECT}} \frac{f_{\mathrm{y}} t_0^2}{\sin\theta} \tag{1}$$

$$Q_{\mathrm{u}} = \frac{2\eta}{(1-\beta)\sin\theta} + \frac{4}{\sqrt{1-\beta}} \tag{2}$$

$$Q_{\mathrm{f,CIDECT}} = (1-|n|)^{C} \tag{3}$$

$$C = \begin{cases} 0.6 - 0.5\beta & \text{for n<0} \\ 0.1 & \text{for n} \geq 0 \end{cases} \tag{4}$$

where Q_{u} is the reference strength equation expressed as a function of brace depth to chord width ratio (η), the brace to chord width ratio (β) and the angle between the brace and chord (θ), f_{y} is the steel yield stress, t_0 is the chord wall thickness, and $Q_{\mathrm{f,CIDECT}}$ is the chord stress equation which accounts for the effect of chord longitudinal stresses, n is the chord preload ratio defined as the ratio of chord preload (N_{p}) to the chord cross-section yield load ($f_{\mathrm{y}}A$). Negative and positive values of n denote compressive and tensile chord axial stresses, respectively. Fig. 11 shows the yield line model on which the CIDECT design strength equations for the RHS X-joints failing by chord face plastification are based [30]. The joint strength can be obtained by equating the external energy by the external force (N_{CIDECT}) over a deflection (δ) (see Fig. 11(a)) and the internal energy by the plastic hinges (No. 1 to 5 in Fig. 11(b)) with yield line lengths (l_{i}) and rotation angles (φ_{i}) as follows:

$$\delta N_{\mathrm{CIDECT}} \sin\theta = \frac{1}{4} f_{\mathrm{y}} t_0^2 \sum l_{\mathrm{i}} \varphi_{\mathrm{i}} \tag{5}$$

The obtained strength equations (N_{CIDECT}) which can generally produce a lower bound strength prediction for the test joint strengths are taken as the characteristic strength equations and the CIDECT design strength equations are derived from the characteristic strength equations divided by a safety factor (γ_{m}) of 1.0 [30], which will be further discussed in Section 5.4. It is noted that the deformation needed to produce the yield line pattern in Fig. 11(b) may be too high for the normal strength steel RHS X-joints with small β ratio, and thus the CIDECT design strength equations yield a lower safety margin for the joints when the indentation limit of 3%b_0 is adopted [30]. The plastic hinges are assumed to reach the yield stresses without considering strain hardening, and the effects of membrane action and weld size are not taken into account. It should also be noted that the chord stress function ($Q_{\mathrm{f,CIDECT}}$) is based on the numerical results for the normal strength steel RHS X-joints obtained by Yu and reanalysis in the CIDECT programmes of 5BK and 5BU [29].

The CIDECT design strength equations for the RHS X-joints with β=1.0 and subjected to brace axial compression which failed by chord side wall failure are as follows:

$$N_{\mathrm{CIDECT,Rd}} = \frac{f_{\mathrm{k}} t_0}{\sin\theta} b_{\mathrm{w}} Q_{\mathrm{f,CIDECT}} \tag{6}$$

$$b_{\mathrm{w}} = 2\left(\frac{h_1}{\sin\theta} + 5t_0\right) \tag{7}$$

$$f_{\mathrm{k}} = 0.8\chi f_{\mathrm{y}} \sin\theta \tag{8}$$

where f_y is the steel yield stress, t_0 is the chord wall thickness, θ is the angle between the brace and chord, h_1 is the brace height, χ is the reduction factor for column buckling according to e.g. the EN 1993-1-1 [31] using the relevant buckling curve and normalised slenderness (λ) determined from:

$$\lambda = 3.46 \frac{\left(\frac{h_0}{t_0} - 2\right)\sqrt{\frac{1}{\sin\theta}}}{\pi\sqrt{\frac{E}{f_{\mathrm{y}}}}} \tag{9}$$

where h_0 is the chord height, E is the elastic modulus. It is noted that the design strength equations are based on the stub column buckling model as illustrated in Fig. 12. The chord side wall is simplified as a pinned-end stub column with thickness of t_0 and height of h_0-2t_0. The column width is taken as $h_1/\sin\theta+5t_0$ to take into account the load which is transferred from the brace height and an alternative load path to the chord side walls through the chord faces. The column buckling stress (f_k) can therefore be obtained from the relevant buckling curves using the normalised slenderness (see Eq. (9)). The coefficient of 0.8 in Eq. (8) is adopted to consider relatively lower ductility of the RHS X-joints which failed by chord side wall failure i.e. a safety factor γ_m=1.25 is incorporated in the design strength equation (Eq. (6)) [32, 33]. It should also be noted that the CIDECT simplified analytical model could result in conservative strength prediction because the chord side wall failure is essentially plate buckling instead of stub column buckling and thus the codified column buckling curves may not be accurate to determine the buckling stresses of chord side walls. The strain hardening and beneficial restraints of the chord faces and the brace member for the chord side walls are also neglected. A linear interpolation between the strength prediction for chord face plastification at β=0.85 and that for chord side wall failure at β=1.0 is adopted by the CIDECT design guide [3] for the RHS X-joints with 0.85<β<1.0 which failed by combined chord face plastification and chord side wall failure.

4.2. Assessment of the CIDECT design rules

4.2.1. General

The applicability of the current CIDECT design rules described in Section 4.1 for the fabricated HSS RHS X-joints was evaluated against the results of the tests in Section 2 and numerical analysis in Section 3.3 in which the indentation limit of 3%b_0 was adopted. To allow for objective and consistent comparison, the CIDECT strength prediction (N_{CIDECT}) was obtained from the CIDECT design strength equations multiplying by the implicit safety factors i.e. γ_m=1.0 for chord face plastification and γ_m=1.25 for chord side wall failure as follows:

$$N_{\mathrm{CIDECT}} = \gamma_{\mathrm{m}} N_{\mathrm{CIDECT,Rd}} \tag{10}$$

Fig. 13 shows the comparison of CIDECT strength prediction (N_{CIDECT}) with numerical strengths obtained in Section 3.3 (N_{FE}) and test strengths summarized in Table 4 (N_{Test}) for the fabricated RHS X-joints without chord preload. Figs. 14-16 show the comparison of the joint strength reduction predicted by Eq. (3) ($Q_{\mathrm{f,CIDECT}}$) with that obtained from the conducted numerical simulations ($Q_{\mathrm{f,FE}}$) for the fabricated RHS X-joints subjected to chord preload. It should be noted that the reduction of joint strength

(Q_f) is defined as the ratio of the static strength of a tubular joint to that of the same joint without chord preload.

4.2.2. RHS X-joints without chord preload

This subsection examines the suitability of the current CIDECT design rules for the fabricated RHS X-joints without chord preload (i.e. $Q_{f,CIDECT}$=1.0). Fig. 13(a)-(c) shows that the comparison of the CIDECT strength prediction (N_{CIDECT}) with the numerical strength (N_{FE}) of the fabricated RHS X-joints (Series 1-8 in Table 7). It is shown that N_{CIDECT}/N_{FE} ratio generally increases with decreasing β ratio and with increasing 2γ ratio and steel grade for the RHS X-joints with $\beta\leq0.85$. Such observations also coincide with the test results as shown in Fig. 13(d). It should be noted that the corresponding CIDECT strength equations are independent of 2γ ratio for $\beta\leq0.85$. However, the test results summarised in Table 4 show that the static strength of the RHS X-joints (X3-X6) decreases from 312 to 172 kN when 2γ ratio increases from 19.8 to 49.1 and therefore demonstrate the significant effect of 2γ ratio. The N_{CIDECT}/N_{FE} ratio generally increases with decreasing 2γ ratio, and the effects of β ratio and steel grade on the N_{CIDECT}/N_{FE} ratio are minor for the RHS X-joints with $0.85<\beta\leq1.0$. Table 8 summarizes the mean values and coefficients of variation (COV) of the N_{CIDECT}/N_{FE} ratio for the analysed RHS X-joints without chord preload. The mean values of N_{CIDECT}/N_{FE} ratio for $0.3\leq\beta\leq0.85$, $0.85<\beta<1.0$ and $\beta=1.0$ are 1.23, 0.68 and 0.52 with corresponding COV of 0.333, 0.154 and 0.525. It is shown that the CIDECT strength prediction is generally unconservative and scattered for the RHS X-joints with $0.3\leq\beta\leq0.85$ and large 2γ ratio, and becomes conservative for $0.85<\beta<1.0$. However, the CIDECT strength prediction is unduly conservative and scattered for $\beta=1.0$.

Fig. 17 illustrates representative load-indentation curves of the fabricated RHS X-joints without chord preload. The applied load in the braces is mainly resisted by the bending action of the chord faces of the RHS X-joints with $\beta\leq0.85$. The corresponding joint strength is generally determined by the load at the indentation limit of 3%b_0 instead of the peak load (i.e. deformation-controlled) as shown in Fig. 17(a)-(c). The deformation of the RHS X-joints using the same steel depends on the joint axial stiffness which increases with increasing β ratio and with decreasing 2γ ratio [34]. The RHS X-joints with larger β ratio and lower 2γ ratio have larger joint stiffness and could be subjected to larger brace loadings and thus higher stresses before the violation of the indentation limit. It is also noted that the yield line model on which the CIDECT strength equations are based assumes that the stresses in the plastic hinges could reach the yield stress (f_y) as discussed in Section 4.1. The increased yield stress of high strength steel could therefore be utilised more effectively in the RHS X-joints with larger β ratio and lower 2γ ratio and thus the corresponding CIDECT strength prediction is generally more accurate and consistent. Fig. 17(a)-(b) shows that relatively large inelastic deformation occurs in the S460 RHS X-joints with low and medium β ratios (i.e. 0.3 and 0.5) at the indentation limit of 3%b_0 while the deformation of the same joints in S690 and S960 steel is largely elastic. Fig. 18 illustrates typical yielding patterns of RHS X-joints with $\beta=0.5$ and $2\gamma=25$ at the determined joint strengths, and the highly strained areas on the chord faces (in red and green colours) almost became plastic. It is shown that the plastic hinges assumed in the yield line model (see Fig. 11(b)) are in the process of developing at the indentation limit for the S460 RHS X-joints. However, the same RHS X-joints in S690 and S960 steel are largely in elastic and the plastic hinges could not be effectively developed. Therefore, the corresponding CIDECT strength prediction becomes increasingly unconservative with increasing steel grade for the RHS X-joints (see Fig. 13). The deformation at the indentation limit becomes largely inelastic for the S460, S690 and S960 RHS X-joints with large β ratio (i.e. 0.8) and the loads at the indentation limit are close to the peak loads as shown in Fig. 17(c). This indicates that the indentation limit is generally not a governing factor limiting the joint strengths, and the yield lines could be developed. The corresponding CIDECT strength prediction is thus relatively accurate (see Fig. 13).

In contrast, the axial compression in the braces of the fabricated RHS X-joints with β ratio approaching or equal to 1.0 is mainly resisted by the chord side walls between the two braces instead of the bending action of the chord faces. The corresponding joint strength is generally determined by the peak load which is controlled by the cross-section yielding or buckling of the chord side walls. Fig. 17(d) shows that the static strengths of the S460, S690 and S960 RHS X-joints with β=1.0 are determined by the peak loads (i.e. strength-controlled), and the improved yield stresses of high strength steel can thus be utilised effectively. However, Fig. 13(a)-(c) shows that the corresponding CIDECT strength prediction is unduly conservative and scattered and becomes increasingly conservative with increasing chord side wall slenderness ($h_0/t_0=b_0/t_0=2\gamma$ for the SHS X-joints). This is mainly because the chord side wall failure is essentially plate buckling instead of stub column buckling, and the strain hardening and beneficial restraints of the chord faces and the brace member for the chord side walls are neglected as discussed in Section 4.1. This also results in the conservative and scattered CIDECT strength prediction for the S460, S690 and S960 RHS X-joints with $0.85<\beta<1.0$ (see Fig. 13(a)-(c)) because of the adopted linear interpolation approach described in Section 4.1.

4.2.3. RHS X-joints with chord preload

This subsection assesses the suitability of the CIDECT chord stress equation (Eq. (3)) for the fabricated RHS X-joints under chord preload. Table 9 summarizes the mean values and COV of the ratio ($Q_{f,CIDECT}/Q_{f,FE}$) of joint strength reduction predicted by the CIDECT chord stress equation (Eq. (3)) ($Q_{f,CIDECT}$) to that obtained in numerical analysis ($Q_{f,FE}$) for the RHS X-joints. The mean values of $Q_{f,CIDECT}/Q_{f,FE}$ ratio for steel grades S460, S690 and S960 are 0.96, 0.94 and 0.93 with corresponding COV of 0.099, 0.099 and 0.112. The comparison of $Q_{f,CIDECT}$ with $Q_{f,FE}$ for the RHS X-joints is also illustrated in Figs. 14-16. The CIDECT prediction of joint strength reduction ($Q_{f,CIDECT}$) is generally conservative and relatively scattered.

Figs. 14-16 show that the effect of chord preload ratio (n) depends on β and 2γ ratios. For the RHS X-joints with small to medium β ratios (e.g. β=0.3, 0.5 and 0.8), the membrane action develops when the chord faces bend resulting in tensile chord axial stresses which can resist the compressive brace loading and thus enhance the joint strength. Enhancement of the joint strength (i.e. $Q_{f,FE}>1.0$) is, therefore, observed in Figs. 14-16 for tensile chord preload while the compressive chord preload generally reduces the joint strength (i.e. $Q_{f,FE}<1.0$). For the RHS X-joints with large β ratio (e.g. β=1.0), the brace loading is mainly resisted by the chord side walls between the two braces. The effect of compressive chord preload on the joint strength is less pronounced while the tensile chord preload lowers the joint strength. This is because a combination of compressive stresses in perpendicular directions results in a higher yield stress than a combination of compressive and tensile stresses according to the von Mises yield criterion [11]. The value of $Q_{f,FE}$ generally decreases with increasing 2γ ratio when n≤0 and with decreasing of 2γ ratio when n>0.

5. Proposed design rules for HSS RHS X-joints

5.1. Chord face plastification

The strength equations for fabricated HSS RHS X-joints which failed by chord face plastification were proposed by modifying the CIDECT strength equations. The analysis described in Section 4.2.2 shows that in general the improved yield stress of HSS could not be fully utilised for the RHS X-joints with small β ratio and large 2γ ratio which failed by chord face plastification mainly due to the adopted indentation limit. The corresponding CIDECT strength prediction is therefore generally unconservative and scattered. It is noted that the CIDECT ranges of β and 2γ ratios are $(0.1+0.02\gamma)\leq\beta\leq0.85$ with a minimum β value of 0.25 and $2\gamma\leq40$, and the cross-section should be class 1 or 2 for the chord members under compression to avoid local buckling of the chord. It is suggested to limit the ranges of β and 2γ ratios to allow for more effective use of HSS in the RHS X-joints. The recommended ranges of β and 2γ ratios are $0.4\leq\beta\leq0.85$ and $2\gamma\leq60\beta-1$, and the cross-section of chord members should be class 1 or 2 when the chord is under compression. The 2γ ratio is tightened for small β ratio e.g. $2\gamma\leq23$ when $\beta=0.4$, but is extended for large β ratio e.g. $2\gamma\leq50$ when $\beta=0.85$. It should be noted that such suggestions are based on the observation that the CIDECT strength predictions are unduly unconservative for the RHS X-joints with β and 2γ beyond the suggested limits as shown in Fig. 13. The recommended parameter ranges can allow for more effective use of the increased yield stress of high strength steel in the RHS X-joints.

The CIDECT strength prediction (N_{CIDECT}) is generally unconservative for the RHS X-joints without chord preload and the joint strength reduction predicted by Eq. (3) ($Q_{\text{f,CIDECT}}$) is conservative and scattered for the RHS X-joints subjected to chord preload when β and 2γ ratios are within the proposed limits (see Figs. 13-16). Regression analysis of numerical results obtained in this study was carried out to propose strength equations for the RHS X-joints using steel grades ranging from S460 to S960 which failed by chord face plastification as follows:

$$N_{\text{Proposed}} = Q_y Q_u Q_{\text{f,Proposed}} \frac{f_y t_0^2}{\sin\theta} \tag{11}$$

$$Q_y = -62 f_y / E + 1.1 \tag{12}$$

$$Q_{\text{f,Proposed}} = (1-|n|)^{C_1} \tag{13}$$

$$C_1 = \begin{cases} 0.50-0.45\beta & \text{for n<0} \\ 0.15 & \text{for } n \geq 0 \end{cases} \tag{14}$$

where Q_y is the proposed reduction factor which accounts for the under-utilisation of the improved yield stresses of HSS, Q_u is the reference strength equation (see Eq. (2)), $Q_{\text{f,Proposed}}$ is the proposed chord stress equation, f_y is the steel yield stress, t_0 is the chord wall thickness, θ is the angle between the brace and chord, E is the elastic modulus, n is the chord preload ratio and β is the brace to chord width ratio. The proposed reduction factors for S460, S690 and S960 steel calculated from Eq. (12) using material properties summarised in Table 6 are 0.96, 0.89 and 0.81, respectively. It should be noted that the proposed reduction factors of joint strength (Q_y) could be conservative for the RHS X-joints with large β ratio and small 2γ ratio (see Fig. 13).

The joint strengths calculated from the proposed strength equations (N_{Proposed}) were compared with the test strengths (N_{Test}) and numerical strengths (N_{FE}) for the RHS X-joints without chord preload. The mean values of the $N_{\text{Proposed}}/N_{\text{Test}}$ and $N_{\text{Proposed}}/N_{\text{FE}}$ ratios summarised in Tables 4 and 8 are 0.60 and 0.85 with corresponding COV of 0.143 and 0.134 for the RHS X-joints with β and 2γ ratios which are within the suggested limits. It is shown that the proposed strength equation (Eq. (11)) can produce somewhat conservative and less scattered strength prediction for the RHS X-joints. The conservative strength equations were proposed to consider the joint strength reduction resulted from the HAZ which could be up to 15% for the RHS X-joints failing by chord face plastification as discussed in Section 3.2. It is noted that the proposed strength prediction becomes more conservative when compared with the test strengths. This is because butt welds with reinforcements were employed for the fabrication of steel tubes and fillet welds were adopted to assemble the brace and chord into the test specimens. However, the finite element model adopted in Section 3.3 excluded the modelling of the reinforcements of the butt welds at the tube corners and the welds connecting the brace and chord were modelled in accordance with the minimum requirements for butt welds specified in AWS D1.1/D1.1M [20], in order to provide lower bound strength prediction for the RHS X-joints in practice. Furthermore, the parameter range of β ratio investigated in the tests is relatively narrow i.e. $0.50 \leq \beta \leq 0.79$.

Figs. 14-16 show the curves of the proposed chord stress equation (Eq. (13)). It is shown that the joint strength reduction predicted by Eq. (13) ($Q_{f,Proposed}$) is more accurate than that obtained from the CIDECT chord stress equation (Eq. (3)) ($Q_{f,CIDECT}$) when compared with the FE results ($Q_{f,FE}$). Table 9 shows that the mean values of the $Q_{f,Proposed}/Q_{f,FE}$ ratio for steel grades S460, S690 and S960 are 0.97, 0.96 and 0.95 with corresponding COV of 0.067, 0.069 and 0.084. It is shown that the proposed chord stress equation is reasonably accurate and slightly conservative. It should be noted that conservative strength equations (Eqs. (11-14)) were proposed for the HSS RHS X-joints in order to consider the joint strength reduction resulted from the HAZ as discussed in Section 3.2. The RHS X-joints with n=-0.8 were not included in the statistical analysis for the $Q_{f,CIDECT}/Q_{f,FE}$ and $Q_{f,Proposed}/Q_{f,FE}$ ratios in Table 9 as such data points may exhibit large errors in percentage terms, in accordance with Lan et al. [11], and those with 2γ=40 and n<0 were also excluded because the majority of RHS X-joints with 2γ=40 and large compressive chord preload (e.g. n=-0.8) failed by local buckling of the chord. Additionally, the RHS X-joints with β<0.4 and 2γ ratio beyond the suggested limit were not included in the statistical analysis for the $Q_{f,Proposed}/Q_{f,FE}$ ratios.

5.2. Chord side wall failure

The analysis described in Section 4.2.2 shows that the CIDECT analytical model could result in unduly conservative and scattered strength prediction for the RHS X-joints with β=1.0 which failed by chord side wall failure. This is mainly because the chord side wall failure which is essentially plate buckling is assumed as stub column buckling, and the beneficial effects of strain hardening and restraints of the chord faces and the brace for the chord side walls are not taken into account. In order to overcome the inherent drawbacks of the CIDECT analytical model, a theoretical model of plate buckling which could consider the beneficial restraints was proposed. The deformation-based continuous strength method (CSM) originally developed for designing non-slender stainless steel cross-sections by Gardner and Nethercot [35] was also adopted to exploit the beneficial effect of strain hardening in the non-slender chord side walls.

Fig. 19 shows the proposed analytical model for chord side wall failure in RHS X-joints. The chord side wall is idealised as a plate under localised stresses (p) from the braces over the intersecting width of $h_1/\sin\theta$ and with plate length of L_0, height of h_0 and thickness of t_0. The restraints of the chord faces and the braces for the chord side walls are stronger than those of pinned-end boundary condition but weaker than those of fixed edges. It is worth noting that Becque and Cheng [36] proposed an analytical model of plate buckling to obtain the elastic buckling stresses (f_{cr}) for equal-width normal strength steel RHS X-joints with β=1.0 and θ=90° as follows:

$$f_{\mathrm{cr,Becque}} = 1.346\frac{\pi^2 E}{12(1-v^2)}\frac{t_0^2}{h_0 h_1} \tag{15}$$

where E is the elastic modulus, v is the Poisson's ratio taken as 0.3 in this study, t_0 is the chord wall thickness, h_0 is the chord height, h_1 is the brace height. It is noted that the chord side walls are assumed to be hinged along the longitudinal edges and made of a linear elastic material without considering the strain hardening effect in the analytical model [36]. The codified column buckling curves were adopted to derive the buckling loads of the chord side walls using a modified imperfection factor of 0.08.

In order to obtain the elastic buckling loads (N_{cr}) of the chord side walls which incorporate the restraint effects of the chord faces and the braces, elastic eigenvalue analysis on the RHS X-joints listed in Table 10 was conducted using the finite element model developed in Section 3.1. The corresponding elastic buckling stress (f_{cr}) was determined by:

$$f_{\mathrm{cr}} = \frac{N_{\mathrm{cr}}}{2t_0 h_1/\sin\theta} \tag{16}$$

Regression analysis of the obtained numerical elastic buckling stresses ($f_{\mathrm{cr,FE}}$) summarised in Table 10 was conducted to derive the expression for the f_{cr} as follows:

$$f_{\mathrm{cr,Proposed}} = 3.2\frac{\pi^2 E}{12(1-v^2)}\left(\frac{t_0}{h_\mathrm{e}}\right)^{1.96}\left(\frac{h_0}{h_1/\sin\theta}\right)^{0.66} \tag{17}$$

where t_0 is the chord wall thickness, h_0 is chord height and h_e is the effective buckling length which is taken as h_0-$2t_0$ for the fabricated RHS X-joints and h_0 for cold-formed and hot-finished steel RHS X-joints to consider the shape effect of chord corners (sharp or round). It is noted that full weld penetration at the junction between the chord side wall and the brace could be difficult to achieve in practice because of the chord round corners in cold-formed and hot-finished steel RHS X-joints [36]. Therefore, the corresponding restraints of the brace for the chord side walls could be weaker resulting in lower elastic buckling stresses, and this is taken into account by suggesting the larger value of h_e (i.e. h_0) for the cold-formed and hot-finished steel RHS X-joints. Table 10 shows the comparison of numerical elastic buckling stresses ($f_{\mathrm{cr,FE}}$) with the calculated elastic buckling stresses ($f_{\mathrm{cr,Becque}}$ and $f_{\mathrm{cr,Proposed}}$). The mean values of $f_{\mathrm{cr,Becque}}/f_{\mathrm{cr,FE}}$ and $f_{\mathrm{cr,Proposed}}/f_{\mathrm{cr,FE}}$ ratios are 0.34 and 1.00 respectively with corresponding COV of 0.123 and 0.032. It is shown that the assumed pinned-edge boundary condition adopted by Becque and Cheng [36] could result in unduly conservative and relatively scattered prediction of the elastic buckling stress for the chord side walls. However, the proposed equation (see Eq. (17)) can provide more accurate and consistent prediction.

The continuous strength method (CSM) was adopted to exploit the beneficial effect of strain hardening for chord side wall failure in RHS X-joints. The numerical results of the fabricated RHS X-joints obtained in Section 3.3 and test results collated from the literature as summarised in Table 11 were used to develop the CSM. The test results include those of RHS X-joints using hot-finished and cold-formed carbon steel [16, 37, 38] and cold-formed stainless steel [39]. It is noted that the base curves and elastic, linear hardening material models are the two key components of the CSM originally developed for designing non-slender stainless steel cross-sections [35], and the CSM has also been extended for the design of non-slender and slender high strength steel tubular sections by Lan et al. [40, 41]. The base curves relate the cross-section deformation capacity to overall cross-section slenderness to consider the element interaction within the cross-section. The overall cross-section slenderness (λ_p) of chord side walls in this study is defined as follows:

$$\lambda_p = \sqrt{\frac{f_y}{f_{cr}}} \tag{18}$$

where f_y is the steel yield stress and f_{cr} is the elastic buckling stress of the chord side walls. Fig. 20 plots the joint strength (N_u) normalised by the yield load (N_y=$2t_0h_1f_y$) of the chord side walls obtained from numerical simulations in Section 3.3 and tests in the literature against the overall cross-section slenderness (λ_p) calculated from Eqs. (17-18). It is shown that the limiting overall cross-section slenderness (λ_p) delineating the transition between non-slender and slender chord side walls approximately equals to 0.68 for the RHS X-joints, which is the same as that for HSS SHS and RHS [40]. The maximum attainable strain (ε_{csm}) in the chord side walls of the analysed fabricated RHS X-joints is defined as:

$$\frac{\varepsilon_{csm}}{\varepsilon_y} = \frac{\delta_u / h_0}{\varepsilon_y} \quad \text{for} \quad \lambda_p \le 0.68 \tag{19}$$

$$\frac{\varepsilon_{csm}}{\varepsilon_y} = \frac{N_u}{N_y} \quad \text{for} \quad \lambda_p > 0.68 \tag{20}$$

where ε_y is the yield strain which equals to f_y/E, δ_u is the chord crown indentation at the ultimate load but not greater than the indentation limit of 3%b_0, h_0 is the chord height, λ_p is the overall cross-section slenderness, N_u is the joint strength, N_y is the yield load of the chord side walls which equals to $2t_0h_1f_y$. It should be noted that the maximum attainable strain should be taken as ε_{csm}=δ_u/h_0-0.002 for steel materials with a round material response (e.g. stainless steel) and ε_{csm}=δ_u/h_0 for those with a sharply defined yield point (e.g. normal strength steel) to be compatible with the adopted CSM material models [40]. Regression analysis of the numerical results obtained in Section 3.3 was conducted to derive the base curves for the RHS X-joints. Fig. 21 shows the proposed base curves for non-slender and slender chord side walls as follows:

$$\frac{\varepsilon_{csm}}{\varepsilon_y} = \frac{0.50}{\lambda_p^{1.80}} \le \min\left(15, \frac{C_1\varepsilon_u}{\varepsilon_y}\right) \quad \text{for} \quad \lambda_p \le 0.68 \tag{21}$$

$$\frac{\varepsilon_{csm}}{\varepsilon_y} = 0.91\left(1 - \frac{0.22}{\lambda_p^{1.60}}\right)\frac{1}{\lambda_p^{1.60}} \quad \text{for} \quad 0.68 < \lambda_p \le 1.78 \tag{22}$$

It is noted that two upper limits ($15\varepsilon_y$ and $C_1\varepsilon_u$) were imposed to the CSM limiting strain (ε_{csm}) (see Eq. (21)) to avoid excessive plastic strain and material fracture for non-slender cross-sections [40]. An upper limit of 1.78 was placed upon the base curves for slender chord side walls as the numerical data have not been examined beyond the upper limit.

The CSM elastic, linear hardening material models adopted by Lan et al. [40] were also employed in this study to obtain the CSM limiting stress (f_{csm}) for the chord side wall failure in the RHS X-joints. For steel materials with round material responses, the CSM bi-linear material model (see Fig. 22(a)) was adopted as follows:

$$f_{csm} = \begin{cases} E\varepsilon_{csm} & \text{for } \varepsilon_{csm} < \varepsilon_y \\ f_y + E_{sh}\left(\varepsilon_{csm} - \varepsilon_y\right) & \text{for } \varepsilon_{csm} \ge \varepsilon_y \end{cases} \tag{23}$$

$$E_{\mathrm{sh}} = \frac{f_{\mathrm{u}} - f_{\mathrm{y}}}{C_2 \varepsilon_{\mathrm{u}} - \varepsilon_{\mathrm{y}}} \tag{24}$$

where E_{sh} is the strain hardening modulus, C_2 is the coefficient defining the strain hardening slope, and ε_{u} is the ultimate strain at ultimate stress which may be determined by:

$$\varepsilon_{\mathrm{u}} = C_3\left(1 - f_{\mathrm{y}}/f_{\mathrm{u}}\right) + C_4 \tag{25}$$

The values of C_1, C_2, C_3 and C_4 reported by Buchanan et al. [42] for various steel materials were adopted herein. The CSM tri-linear material model i.e. the first three stages of the quad-linear stress-strain curve model for hot-rolled steel proposed by Yun and Gardner [43] (see Fig. 22(b)) was employed for steel with a sharply defined yield point as follows:

$$f_{\mathrm{csm}} = \begin{cases} E\varepsilon & \text{for } \varepsilon \le \varepsilon_{\mathrm{y}} \\ f_{\mathrm{y}} & \text{for } \varepsilon_{\mathrm{y}} < \varepsilon \le \varepsilon_{\mathrm{sh}} \\ f_{\mathrm{y}} + E_{\mathrm{sh}}\left(\varepsilon - \varepsilon_{\mathrm{sh}}\right) & \text{for } \varepsilon_{\mathrm{sh}} < \varepsilon \le C_1\varepsilon_{\mathrm{u}} \end{cases} \tag{26}$$

$$C_1 = \frac{\varepsilon_{\mathrm{sh}} + 0.25\left(\varepsilon_{\mathrm{u}} - \varepsilon_{\mathrm{sh}}\right)}{\varepsilon_{\mathrm{u}}} \tag{27}$$

$$\varepsilon_{\mathrm{sh}} = 0.1\frac{f_{\mathrm{y}}}{f_{\mathrm{u}}} - 0.055 \quad \text{but } 0.015 \le \varepsilon_{\mathrm{sh}} \le 0.03 \tag{28}$$

$$\varepsilon_{\mathrm{u}} = 0.6\left(1 - \frac{f_{\mathrm{y}}}{f_{\mathrm{u}}}\right) \quad \text{but } \varepsilon_{\mathrm{u}} \ge 0.06 \tag{29}$$

$$E_{\mathrm{sh}} = \frac{f_{\mathrm{u}} - f_{\mathrm{y}}}{0.4\left(\varepsilon_{\mathrm{u}} - \varepsilon_{\mathrm{sh}}\right)} \tag{30}$$

where C_1 is the material coefficient and $\varepsilon_{\mathrm{sh}}$ is the strain-hardening strain.

The static strength of the chord side wall failure in the equal-width RHS X-joints under brace axial compression (N_{Proposed}) can be determined from:

$$N_{\mathrm{Proposed}} = \frac{f_{\mathrm{csm}} t_0}{\sin\theta}\left(2h_1 + a_1 t_0\right) Q_{\mathrm{f,Proposed}} \qquad \text{for } \lambda_{\mathrm{p}} \le 0.68 \tag{31}$$

$$N_{\mathrm{Proposed}} = \frac{\varepsilon_{\mathrm{csm}}}{\varepsilon_{\mathrm{y}}} \frac{f_{\mathrm{y}} t_0}{\sin\theta}\left(2h_1 + a_2 t_0\right) Q_{\mathrm{f,Proposed}} \qquad \text{for } 0.68 < \lambda_{\mathrm{p}} \le 1.78 \tag{32}$$

where the terms of $a_1 t_0$ and $a_2 t_0$ are employed to consider the load transferred from an alternative load path to the chord side walls through the chord faces, and $Q_{\mathrm{f,Proposed}}$ is the proposed chord stress function (see Eq. (13)). Regression analysis of the numerical and test results using the proposed base curves (Eqs. (21-22)) and the adopted CSM material models was conducted to derive the coefficients of a_1 and a_2. It is suggested that a_1=a_2=8 for the fabricated RHS X-joints with sharp chord corners, and a_1=6 and a_2=0 for the hot-finished and cold-formed RHS X-joints with round chord corners. It is noted the validity range of the design rules for the RHS X-joints specified in the CIDECT design guide [3] is $2\gamma \le 40$ and the proposed design method is applicable for 2γ ratio up to 50.

Table 8 shows that the mean value of the $N_{\mathrm{Proposed}}/N_{\mathrm{FE}}$ ratio for the fabricated equal-width RHS X-joints with β=1.0 is 0.92 with corresponding COV of 0.076. It is shown that the proposed design method herein can produce slightly conservative and consistent strength prediction for the fabricated RHS X-joints. The conservative strength equations were proposed to consider the joint strength reduction resulted from the HAZ which could be up to 8% for the RHS X-joints failing by chord side wall failure as discussed in Section 3.2. The joint strengths obtained from the CIDECT design guide [3] (N_{CIDECT}) and those determined from Becque and Cheng [36] (N_{Becque}) and the proposed design method herein ($N_{Proposed}$) were also compared with the test strengths in the literature (N_{Test}) as shown in Table 11. It should be noted that the values of ultimate stresses (f_u) which were not reported in Packer et al. [37] were taken as $1.1f_y$ in accordance with the minimum ductility requirements stipulated in EN 1993-1-1 [31] (i.e. $f_u/f_y \geq 1.10$) and the elastic modulus (E) was taken as 210 GPa [31] for the specimens tested by Packer et al. [37] and Cheng and Becque [38]. It is also noted that the design method proposed by Becque and Cheng [36] is only applicable for the RHS X-joints with θ=90°, and thus the RHS X-joints with θ<90° were not included for the analysis of the N_{Becque}/N_{Test} ratio in Table 11. The mean values of the N_{CIDECT}/N_{Test}, N_{Becque}/N_{Test} and $N_{Proposed}/N_{Test}$ ratios for the cold-formed and hot-finished steel RHS X-joints are 0.46, 0.60 and 0.99 with corresponding COV of 0.417, 0.253 and 0.075. The strength predictions of the CIDECT design guide [3] and Becque and Cheng [36] are conservative and scattered while the proposed design method is shown to be also applicable for the cold-formed and hot-finished steel RHS X-joints. Fig. 23 further illustrates the comparison of numerical and test joints strengths (N_u) with the predicted strengths ($N_{u,pred}$). It is shown that the strength predictions of the CIDECT design guide [3] and Becque and Cheng [36] are unduly and increasingly conservative with increasing chord side wall slenderness except for some X-joints with small chord side wall slenderness. However, the proposed design method can produce slightly conservative and consistent strength prediction. It should be noted that the proposed design method may also be applicable for other RHS tubular joints failing by chord side wall failure (e.g. RHS T- and Y-joints) and RHS members which failed by web crippling. It may provide a unified design framework for these tubular joints and tubular members using various steel materials e.g. normal and high strength carbon steel, stainless steel and aluminium alloys. Related research work is currently underway.

5.3. Combined failure modes

The analysis in Section 4.2.2 shows that the CIDECT strength prediction is generally conservative and scattered for the RHS X-joints with 0.85<β<1.0 which failed by combined chord face plastification and chord side wall failure. This is because the CIDECT strength predictions at β=0.85 and β=1.0 are conservative and scattered, and a linear interpolation approach is adopted by the CIDECT design guide [3] for the RHS X-joints with 0.85<β<1.0. The proposed strength equations for the RHS X-joints with $\beta \leq$0.85 (Eq. (11)) and those with β=1.0 (Eqs. (31-32)) can provide more accurate and consistent strength predictions, and therefore the linear interpolation approach using the proposed strength equations at β=0.85 and β=1.0 is also suggested for the RHS X-joints with 0.85<β<1.0. Table 8 shows that the adopted linear interpolation approach can produce slightly conservative and consistent strength prediction with a mean value of $N_{Proposed}/N_{FE}$ ratio of 0.91 and corresponding COV of 0.072. Therefore, the linear interpolation approach is also applicable for the fabricated RHS X-joints. It should be noted that validity ranges of the proposed design approach are 0.85<β<1.0 and 2$\gamma \leq$50.

5.4. Determination of design strengths

The 3rd edition of IIW recommendations [28] on which the current CIDECT design guide [3] is based adopts a two-step procedure to obtain the design strength i.e. firstly converts the mean strength to the characteristic strength, and then derives the design strength from the characteristic strength divided by a safety factor. The regression analysis of test or numerical data for the reference strength equation (Q_u) and the chord stress equation (Q_f) leads to the mean strength equations. The mean strength equation can be converted to the characteristic strength equation by considering fabrication tolerances, mean values and scatter of test or numerical data and a correction of steel yield stress [11, 32]. The design strength equation can be derived from the characteristic strength equation divided by a safety factor. It is noted that the CIDECT analytical models for the RHS X-joints which failed by chord face plastification and chord side wall failure can produce lower bound strength predictions for test strengths of normal strength steel RHS X-joints [32]. The analytical equations derived from the theoretical models are therefore taken as the characteristic strength equations in the IIW recommendations [28] and the CIDECT design guide [3]. The safety factors (γ_m) adopted by the CIDECT design guide [3] are 1.0 for chord face plastification and 1.25 for chord side wall failure (see Table C.1 in ISO 14346 [33]). This is because the RHS X-joints which failed by chord face plastification in tests have demonstrated sufficient ductility and the adopted analytical model can give a lower bound strength prediction. However, the RHS X-joints failing by chord side wall failure have relatively lower ductility and less plasticity, and thus a safety factor of 1.25 was employed by incorporating the coefficient of 0.8 in the buckling stress equation (see Eq. (8)) [32]. It should be noted that the approach adopted by the IIW recommendations [28] differs from that used by current design codes e.g. Eurocode EN 1990 [44] and ASCE Standard [45] which derive the design strength equation directly from the nominal strength equation divided by a partial factor. The nominal strength equation is generally obtained from theoretical analysis and regression analysis of test and numerical results.

The procedure adopted by the IIW recommendations [28] was employed herein to derive the design strength equations. It is noted that the proposed strength equations (see Eq. (11) and Eqs. (31-32)) for RHS X-joints are based on the analytical models which can provide reasonably accurate and consistent lower bound strength predictions when compared with the test strengths (see Table 4) and numerical strengths (see Tables 8-9). Eq. (11) and Eqs. (31-32) can therefore be adopted as the characteristic strength equations for the RHS X-joints which failed by chord face plastification and chord side wall failure respectively. The tests conducted in this study have demonstrated that the deformation capacity and ductility of the test specimens which failed by chord face plastification are sufficient (see Figs. 6-7). Fig. 17(d) shows that the load drops significantly after the peak load which therefore indicates the lower ductility of the RHS X-joints failing by chord side wall failure. Safety factors of 1.0 and 1.25 are thus suggested for chord face plastification and chord side wall failure respectively to derive the corresponding design strength equations, in line with the recommendations of the IIW recommendations [28]. The design strengths of the combined failure modes can be obtained from the linear interpolation approach using the derived design strength equations at β=0.85 and β=1.0.

It should be noted that the range of 2γ ratio is suggested to be tightened for the fabricated RHS X-joints with small β ratio which failed by chord face plastification to allow for more effective use of HSS. Reinforcements such as internal ring stiffeners [46, 47], external stiffeners [48] and grouting concrete [49, 50] can be employed for the RHS X-joints with small β ratio and large 2γ ratio to enhance the joint stiffness and thus to utilise the HSS more effectively. Investigations on the HSS reinforced tubular joints are needed.

6. Conclusions

The structural behaviour and static strength of fabricated RHS X-joints using steel grades ranging from S460 to S960 and under axial compression in the braces were investigated through tests and numerical analysis. Eight RHS X-joints which were composed of fabricated steel tubes with a measured yield stress of 907 MPa were tested, and totally 599 numerical simulations on the RHS X-joints were conducted. The investigated failure modes are chord face plastification, chord side wall failure and a combination of these two failure modes. The effects of heat affected zones (HAZ) and suitability of the strength equations adopted by the CIDECT design guide for the RHS X-joints were examined. Influences of the steel grade, brace to chord width ratio (β), chord width to wall thickness ratio (2γ) and chord preload on the applicability of the CIDECT strength equations for the RHS X-joints were also assessed. Design rules were proposed for RHS X-joints. The conclusions are summarized as follows:

(1) The test specimens failed by chord face plastification. The corresponding chord face indentation and chord side deformation could reach at least two times of the CIDECT indentation limit of 3% of chord width, and brittle failure was not observed at large deformations. The deformation capacity when compared with the CIDECT indentation limit and ductility of the test specimens could be considered as reasonably sufficient.

(2) The effect of material strength reduction in HAZ on the initial stiffness of the RHS X-joints is minor. However, the effect can be more significant for the joint strength. The joint strength reduction resulted from the HAZ can be more pronounced for the RHS X-joints with medium β ratio than those with small or large β ratio.

(3) The CIDECT strength prediction is, in general, increasingly unconservative with increasing steel grade and 2γ ratio and with decreasing β ratio for the RHS X-joints failing by chord face plastification. However, it is conservative for the combined failure modes, and becomes increasingly conservative with increasing chord side wall slenderness for chord side wall failure. The CIDECT prediction of joint strength reduction resulted from the chord preload is relatively conservative.

(4) High strength steel generally cannot be fully utilised for the RHS X-joints with small β ratio and large 2γ ratio failing by chord face plastification mainly due to the adopted indentation limit. The CIDECT strength prediction for the combined failure modes and chord side wall failure is conservative because the chord side wall failure is assumed as column buckling and the beneficial effects of strain hardening and restraints of the brace and chord faces for the chord side walls are neglected.

(5) The suggested ranges of β and 2γ ratios are $0.4 \leq \beta \leq 0.85$ and $2\gamma \leq 60\beta-1$ for the RHS X-joints failing by chord face plastification to allow for more effective use of high strength steel, and corresponding accurate and slightly conservative strength equations were proposed.

(6) An analytical model of plate buckling was proposed and the deformation-based continuous strength method was adopted for designing chord side wall failure in the RHS X-joints with β=1.0 and 2γ up to 50. The proposed design method is also applicable for designing chord side wall failure in equal-width RHS X-joints using cold-formed and hot-finished carbon steel and cold-formed stainless steel.

(7) A linear interpolation approach using the proposed strength equations at β=0.85 and β=1.0 is suggested for the RHS X-joints with $0.85<\beta<1.0$ and $2\gamma \leq 50$ which failed by a combination of chord face plastification and chord side wall failure.

(8) The proposed strength equations can produce more accurate and consistent strength prediction than the current CIDECT design rules, and were converted to design strength equations for designing high strength steel RHS X-joints.

Acknowledgements

The authors appreciate the support from the Chinese National Engineering Research Centre for Steel Construction (Hong Kong Branch) at The Hong Kong Polytechnic University and the research seed funds from The Hong Kong Polytechnic University (PolyU/1-ZE50/G-YBUU). The first author is also grateful for the support given by the Research Grants Council of Hong Kong for the Hong Kong PhD Fellowship Scheme.

References

[1] X.Y. Lan, T.M. Chan, Recent research advances of high strength steel welded hollow section joints, Struct. 17 (2019) 58-65.

[2] Eurocode 3 (EC3), Design of steel structures-Part 1–8: Design of joints. European Committee for Standardization, EN 1993-1-8, CEN, Brussels, 2005.

[3] J.A. Packer, J. Wardenier, X.L. Zhao, G.J. van der Vegte, Y. Kurobane, Design guide for rectangular hollow section (RHS) joints under predominantly static loading, CIDECT, Verlag TUV Rheinland, Cologne, Germany, 2009.

[4] J. Wardenier, Y. Kurobane, J.A. Packer, G.J. van der Vegte, X.L. Zhao, Design guide for circular hollow section (CHS) joints under predominantly static loading, CIDECT, Verlag TUV Rheinland, Cologne, Germany, 2008.

[5] EN 1993-1-12, Eurocode 3: Design of steel structures-Part 1–12: Additional rules for the extension of EN 1993 up to steel grades S700, European Committee for Standardization, EN 1993-1-12, CEN, Brussels, 2007.

[6] D.K. Liu, J. Wardenier, Effect of the yield strength on the static strength of uniplanar K-Joints in RHS (Steel Grade S460, S355 and S235), IIW Doc. XV-E-04-293, 2004.

[7] Y. Kurobane, New development and practices in tubular joint design, IIW Doc. XV-448-81 and IIW Doc. XIII-1004-81, 1981.

[8] R. Puthli, O. Bucak, S. Herion, O. Fleischer, A. Fischl, O. Josat, Adaptation and extension of the valid design formulae for joints made of high-strength steels up to S690 for cold-formed and hot-rolled sections, CIDECT Report 5BT-7/10 (Draft Final Report), CIDECT, Germany, 2011.

[9] C.H. Lee, S.H. Kim, D.H. Chung, D.K. Kim, J.W. Kim, Experimental and numerical study of cold-formed high-strength steel CHS X-joints, J. Struct. Eng. 143 (8) (2017), 04017077.

[10] X.Y. Lan, T.M. Chan, B. Young, Static strength of high strength steel CHS X-joints under axial compression, J. Constr. Steel Res. 138 (2017) 369–379.

[11] X.Y. Lan, T.M. Chan, B. Young, Structural behaviour and design of chord plastification in high strength steel CHS X-joints, Constr. Build. Mater. 191 (2018), 1252-1267.

[12] J. Becque, T. Wilkinson, The capacity of grade C450 cold-formed rectangular hollow section T and X connections: an experimental investigation, J. Constr. Steel Res. 133 (2017) 345–359.

[13] M. Mohan, T. Wilkinson, Finite element simulations of 450 grade cold-formed K and N joints, Tubular Structures XV, CRC Press, Brazil 2015, pp. 449–456.

[14] J. Havula, M. Garifullin, M. Heinisuo, K. Mela, S. Pajunen, Moment-rotation behavior of welded tubular high strength steel T joint, Eng. Struct. 172 (2018) 523–537.

[15] M. Feldmann, N. Schillo, S. Schaffrath, K. Virdi, T. Björk, N. Tuominen, M. Veljkovic, M. Pavlovic, P.

Manoleas, M. Heinisuo, K. Mela, P. Ongelin, I. Valkonen, J. Minkkinen, J. Erkkilä, E. Pétursson, M. Clarin, A. Seyr, L. Horváth, B. Kövesdi, P. Turán, B. Somodi, Rules on high strength steel, Luxembourg, Publications Office of the European Union, 2016.

[16] M. Pandey, B. Young, High strength steel tubular X-joints-an experimental insight under axial compression, Tubular Structures XV, CRC Press, Melbourne 2017, pp. 223–230.

[17] X.Y. Lan, Y Huang, Structural design of cold-formed stainless steel tubular X-and T-joints at elevated temperatures, Thin Wall. Struct. 108 (2016) 270–279.

[18] ISO. Metallic materials-Tensile testing-Part 1: Method of test at room temperature. ISO 6892-1: 2009(E), Switzerland.

[19] ASTM. Standard test methods for tension testing of metallic materials. ASTM E8/E8M: 2016, United States.

[20] AWS. Structural welding code-steel. AWS D1.1/D1.1M: 2010, United States.

[21] SSAB. Welding handbook-A guide to better welding of Hardox and Weldox, 2009, Sweden.

[22] Abaqus/Standard. Version 6.13-1. USA: K. a. S. Hibbit; 2013.

[23] R. Stroetmann, Thoralf Kastner, A. Halsig, P. Mayr, Mechanical properties and a new design approach for welded joints at high strength steels, Engineering Research and Practice for Steel Construction, Hong Kong 2018, pp. 79–90.

[24] J. Siltanen, S. Tihinen, J. Kömi, Laser and laser gas-metal-arc hybrid welding of 960 MPa direct-quenched structural steel in a butt joint configuration, J. Laser Appl. 27(S2) (2015) S29007.

[25] F. Javidan, A. Heidarpour, X.L. Zhao, C.R. Hutchinson, J. Minkkinen, Effect of weld on the mechanical properties of high strength and ultra-high strength steel tubes in fabricated hybrid sections, Eng. Struct. 118 (2016) 16–27.

[26] H. Ban, G. Shi, Overall buckling behaviour and design of high-strength steel welded section columns, J. Constr. Steel Res. 143 (2018) 180–195.

[27] International Institute of Welding (IIW) Subcommission XV-E, IIW Doc. XV-701-89: Design recommendations for hollow section joints–predominantly statically loaded, 2nd Ed., IIW, Paris, 1989.

[28] International Institute of Welding (IIW) Subcommission XV-E, IIW Doc. XV-1329-09: Static Design Procedure for Welded Hollow Section Joints–Recommendations, 3rd Ed., IIW, Singapore, 2009.

[29] J. Wardenier, J.A. Packer, X.L. Zhao, G.J. van der Vegte, Background of the new RHS joint strength equations in the IIW (2009) recommendations, Tubular Structures XIII, CRC Press, Leiden 2010, pp.403–412.

[30] J. Wardenier, Hollow sections in structural applications, 2nd Ed., CIDECT, Geneva, 2011.

[31] Eurocode 3 (EC3), Design of Steel Structures–Part 1–1: General Rules and Rules for Buildings. European Committee for Standardization, EN 1993-1-1, CEN, Brussels, 2005.

[32] J. Wardenier, Hollow Section Joints, Delft University Press, The Netherlands, 1982.

[33] ISO. Static design procedure for welded hollow-section joints-Recommendations. ISO/FDIS 14346: 2012(E), Geneva.

[34] M. Garifullin, M. Bronzova, S. Pajunen, K. Mela, M. Heinisuo, Initial axial stiffness of welded RHS T joints, J. Constr. Steel Res. 153 (2019) 459–472.

[35] Gardner L, Nethercot D. Structural stainless steel design: a new approach. Struct Eng 2004; 82: 2-28.

[36] J. Becque, S. Cheng, Sidewall buckling of equal-width RHS truss X-joints, J. Struct. Eng. 143(2) (2016) 04016179.

[37] J.A. Packer, Web crippling of rectangular hollow sections, J. Struct. Eng. 110(10) (1984) 2357-2373.

[38] S. Cheng, J. Becque, A design method for side wall failure of RHS truss X-joints accounting for

compressive chord pre-load, Eng. Struct. 126 (2016) 689-702.
[39] R. Feng, B. Young, Design of cold-formed stainless steel tubular T-and X-joints, J. Constr. Steel Res. 67(3) (2011) 421-436.
[40] X.Y. Lan, J.B. Chen, T.M. Chan, B. Young, The continuous strength method for the design of high strength steel tubular sections in compression, Eng. Struct. 162 (2018) 177-187.
[41] X.Y. Lan, J.B. Chen, T.M. Chan, B. Young, The continuous strength method for the design of high strength steel tubular sections in bending, J. Constr. Steel Res. https://doi.org/10.1016/j.jcsr.2019.05.037.
[42] C. Buchanan, L. Gardner, A. Liew, The continuous strength method for the design of circular hollow sections, J. Constr. Steel Res. 118 (2016) 207–216.
[43] X. Yun, L. Gardner, Stress-strain curves for hot-rolled steels, J. Constr. Steel Res. 133 (2017) 36–46.
[44] Eurocode, Basis of structural design. European Committee for Standardization, EN 1990, CEN, Brussels, 2002.
[45] American Society of Civil Engineers (ASCE) Standard, Minimum design loads for buildings and other structures. ASCE/SEI 7-05, New York, 2006.
[46] X.Y. Lan, F. Wang, C. Ning, X.F. Xu, X.R. Pan, Z.F. Luo, Strength of internally ring-stiffened tubular DT-joints subjected to brace axial loading, J. Constr. Steel Res. 125 (2016) 88–94.
[47] X.Y. Lan, F. Wang, Z.F. Luo, D.D. Liu, C. Ning, X.F. Xu, Joint strength reduction factor of internally ring-stiffened tubular joints at elevated temperatures, Adv. Struct. Eng. 19(10) (2016) 1650–1660.
[48] W. Li, S. Zhang, W. Huo, Y. Bai, L. Zhu, Axial compression capacity of steel CHS X-joints strengthened with external stiffeners, J. Constr. Steel Res. 141 (2018) 156–166.
[49] H.T. Li, B. Young, Experimental investigation of concrete-filled high-strength steel tubular X joints, J. Struct. Eng. 144(10) (2018) 04018178.
[50] H.T. Li, B. Young, Design of concrete-filled high strength steel tubular joints subjected to compression, J. Constr. Steel Res. 150 (2018) 209–220.

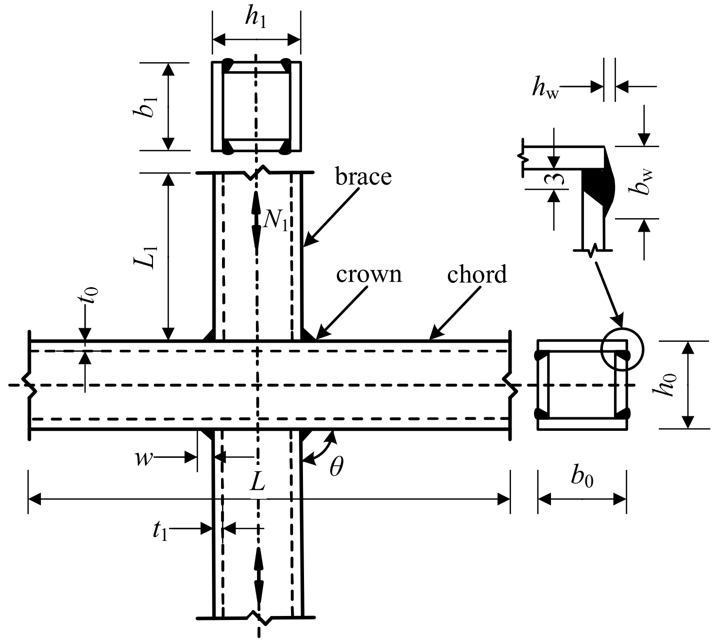

Fig. 1. Configuration and notations of fabricated RHS X-joints (dimensions in mm).

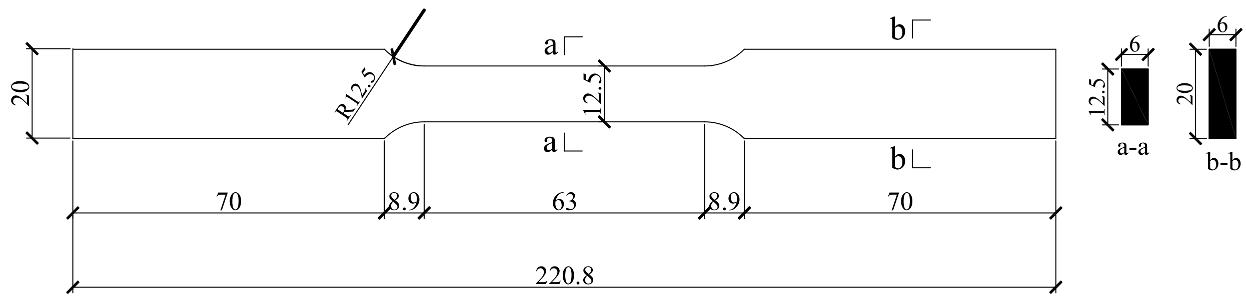

Fig. 2. Dimensions of flat tensile coupons (dimensions in mm).

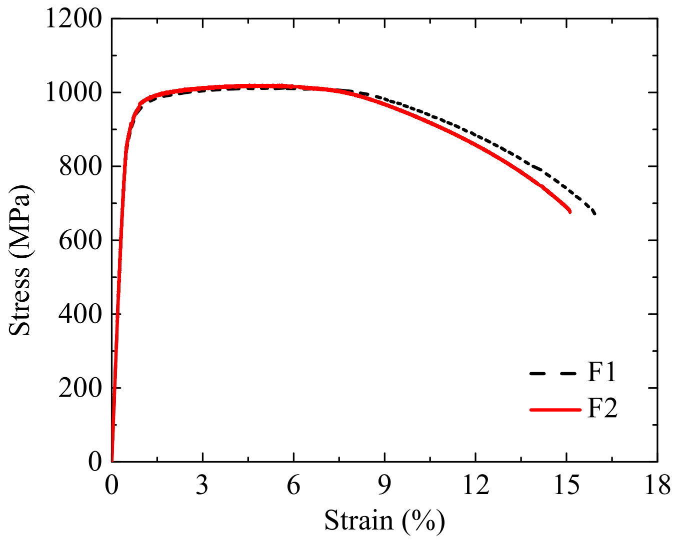

Fig. 3. Static engineering stress-strain curves of high strength steel obtained from tensile coupon tests.

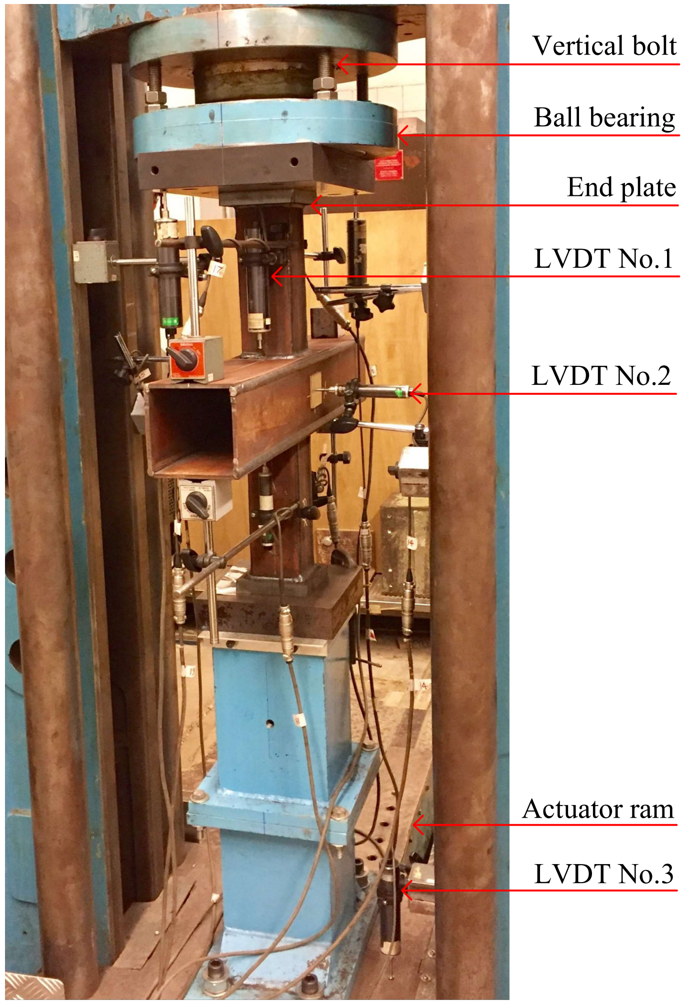

Fig. 4. Test set-up for high strength steel RHS X-joint specimens.

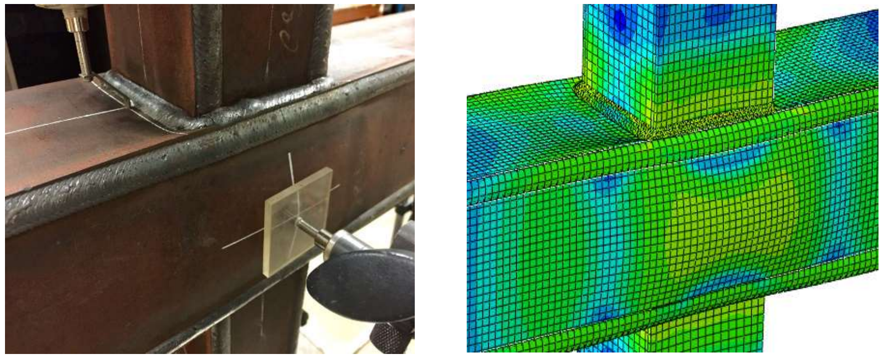

(a) Specimen X1#

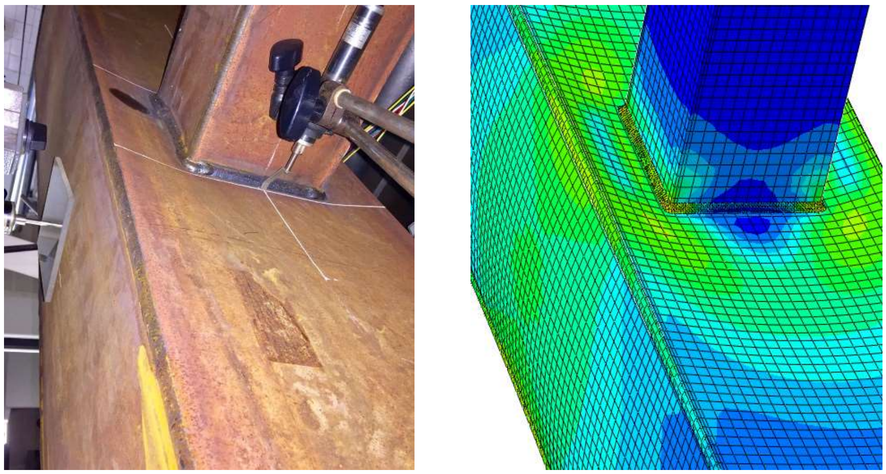

(b) Specimen X6

Fig. 5. Experimental and numerical failure modes of high strength steel RHS X-joint specimens.

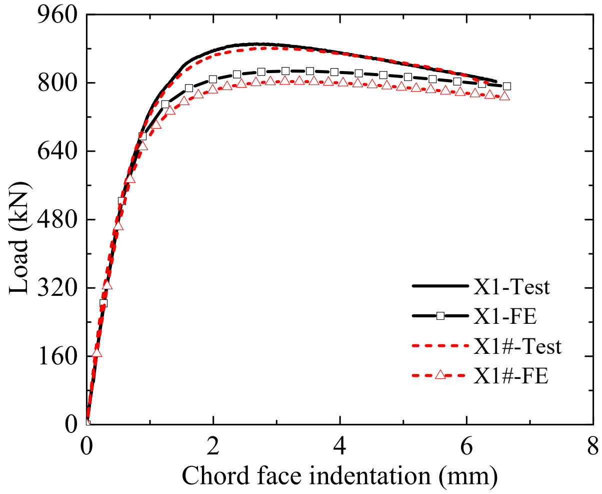

(a) Specimens X1 and X1#

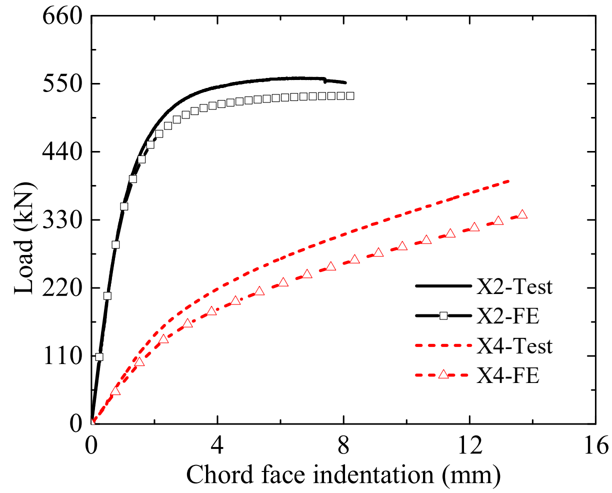

(b) Specimens X2 and X4

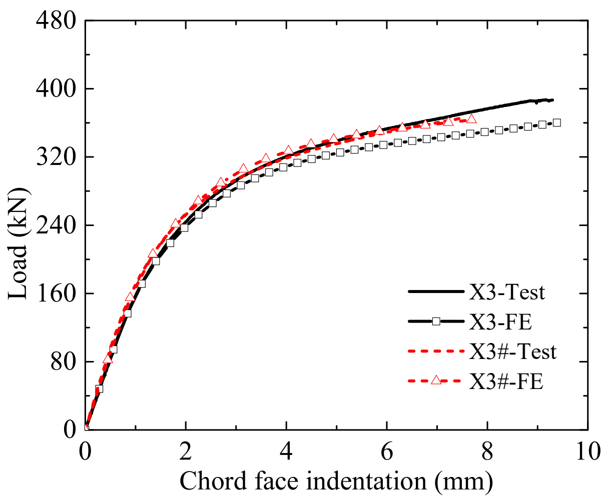

(a) Specimens X3 and X3#

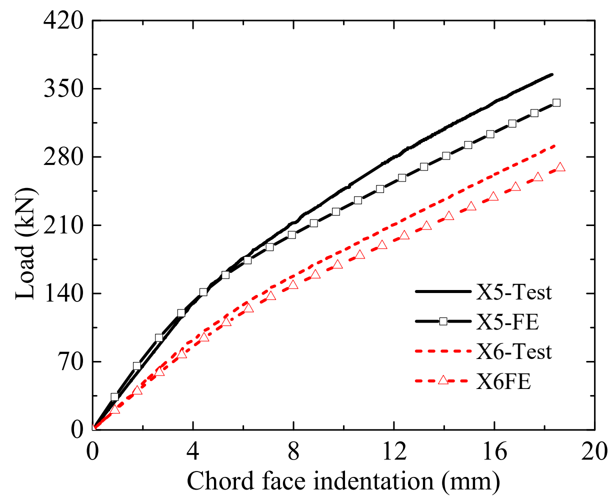

(b) Specimens X5 and X6

Fig. 6. Test and FE load-chord face indentation curves of high strength steel RHS X-joint specimens.

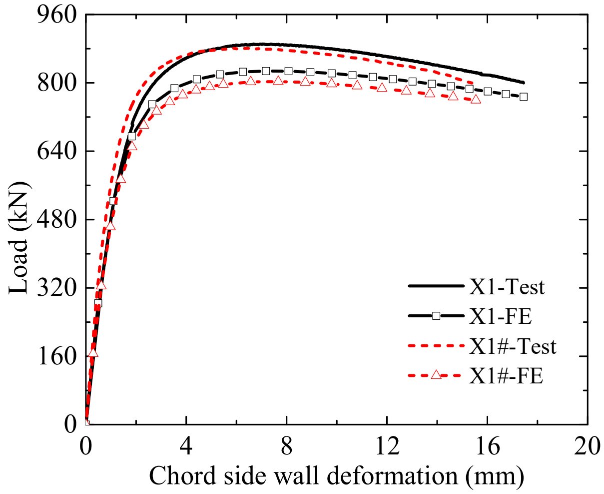

(a) Specimens X1 and X1#

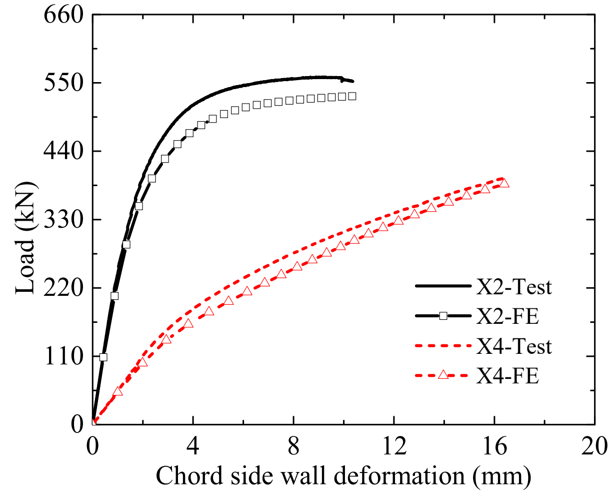

(b) Specimens X2 and X4

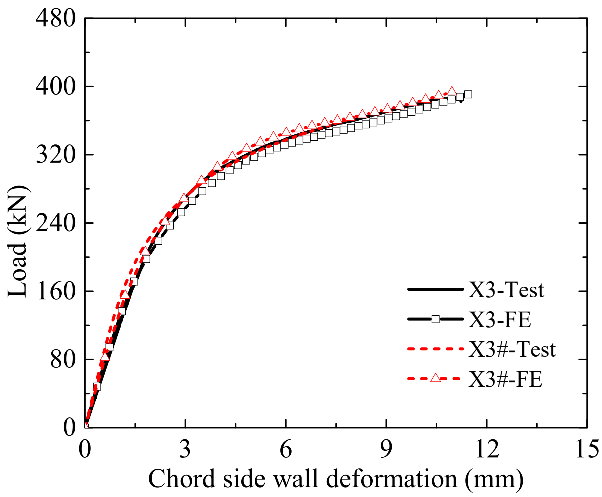

(a) Specimens X3 and X3#

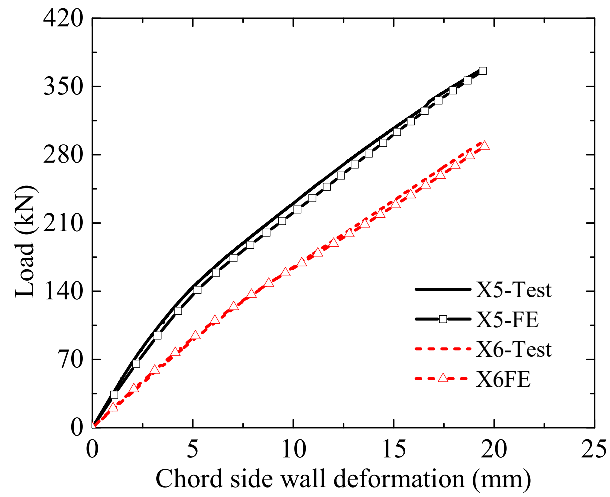

(b) Specimens X5 and X6

Fig. 7. Test and FE load-chord side wall deformation curves of high strength steel RHS X-joint specimens.

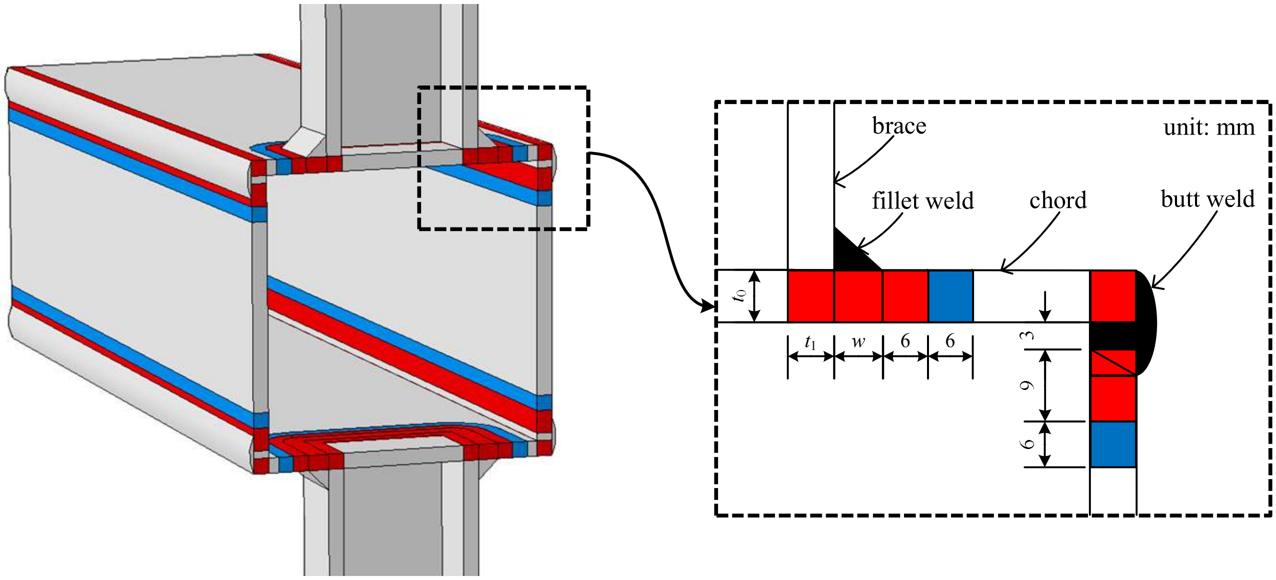

Fig. 8. Heat affected zones in S960 steel RHS X-joints (20% and 10% material strength reduction in red and blue regions respectively).

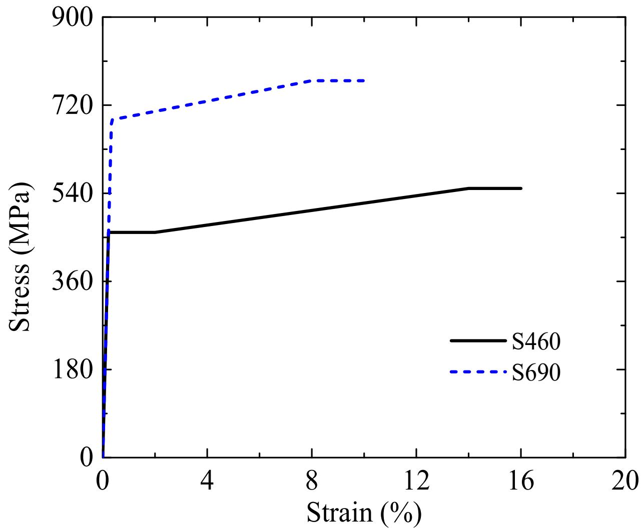

(a) S460 and S690

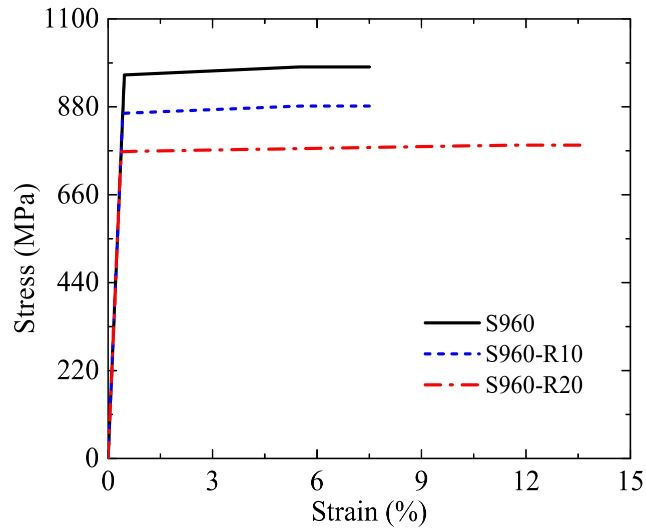

(b) S960

Fig. 9. Engineering stress-strain curves of high strength steel.

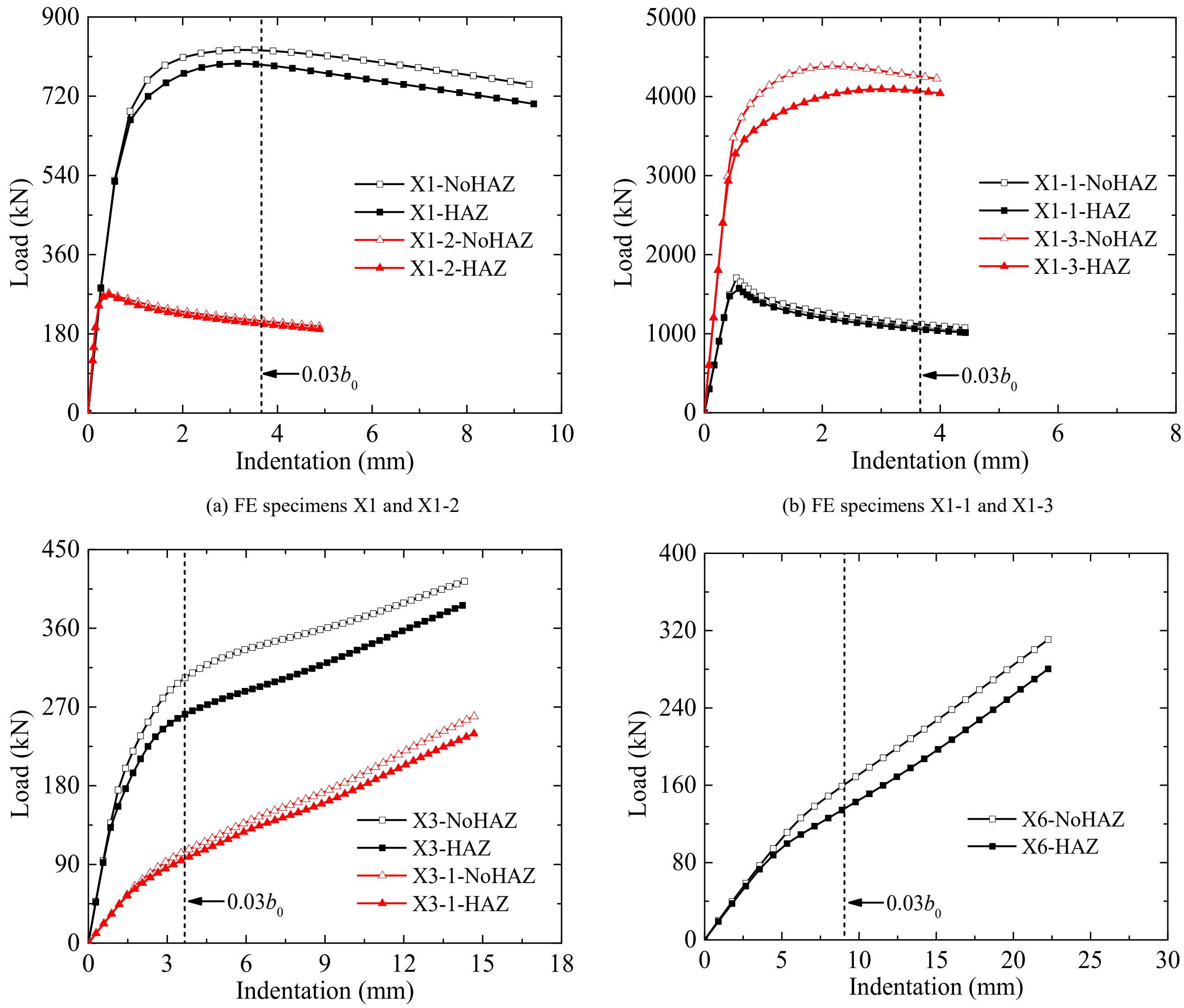

(a) FE specimens X1 and X1-2

(b) FE specimens X1-1 and X1-3

(c) FE specimens X3 and X3-1

(d) FE specimen X6

Fig. 10. FE load-indentation curves of fabricated S960 steel RHS X-joints without and with HAZ.

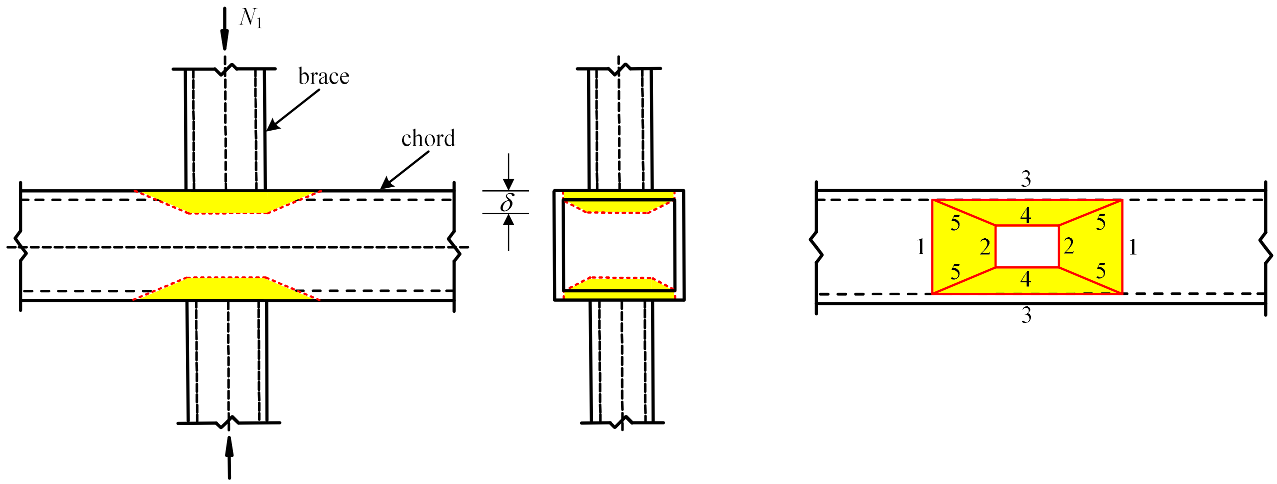

(a) Assumed deformation configuration (b) Yield lines on top and bottom chord faces

Fig. 11. CIDECT analytical model for chord face plastification in RHS X-joints.

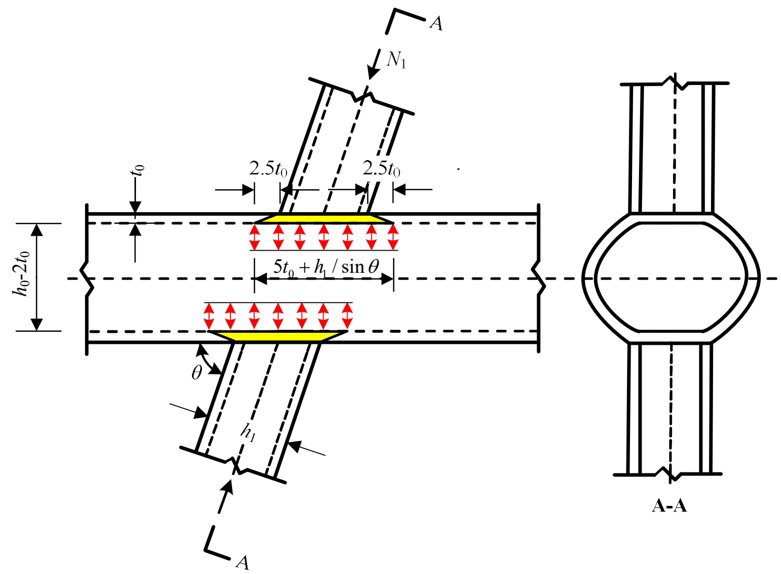

Fig. 12. CIDECT analytical model for chord side wall failure in RHS X-joints.

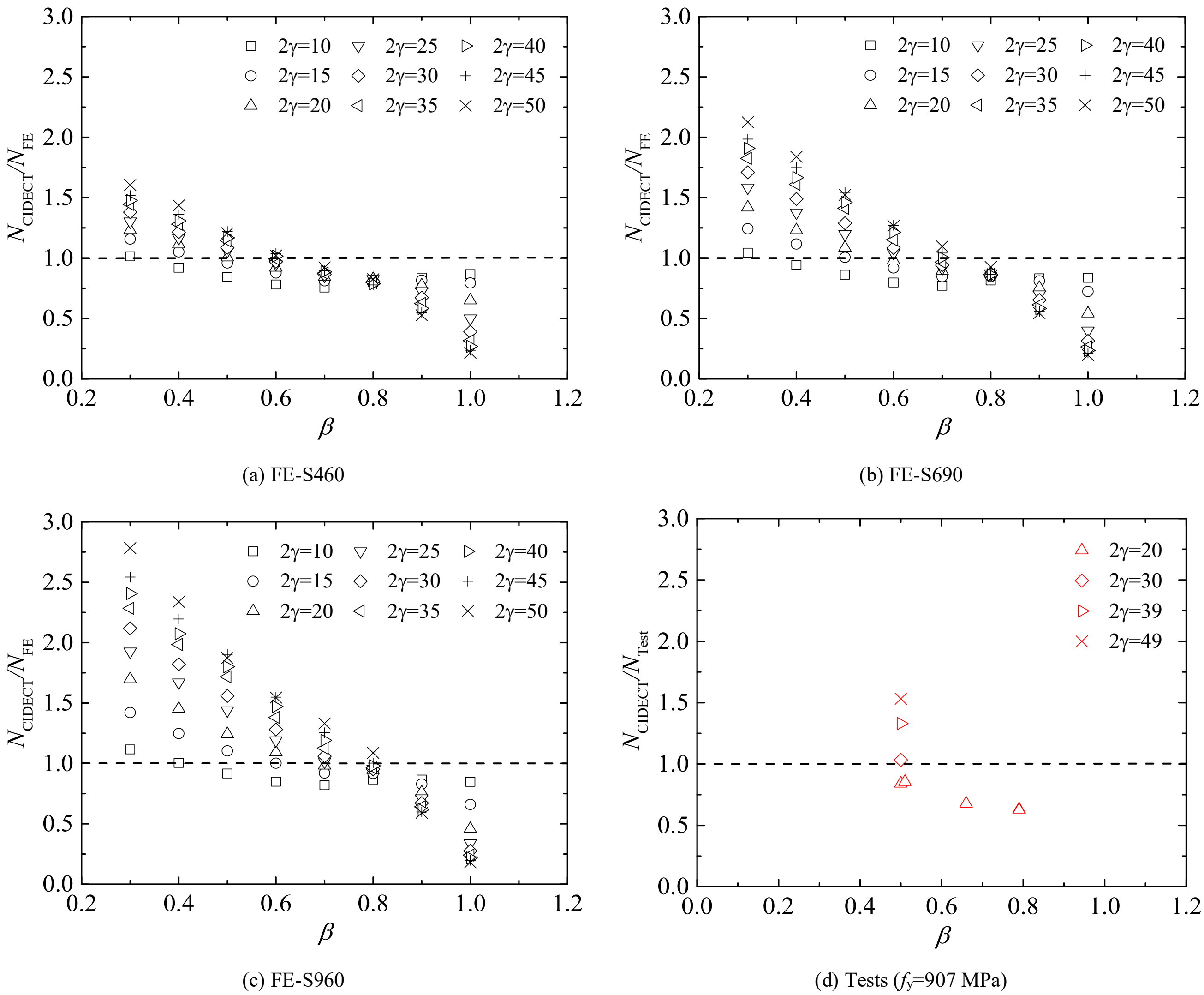

Fig. 13. Comparison of joint strengths for fabricated RHS X-joints without chord preload.

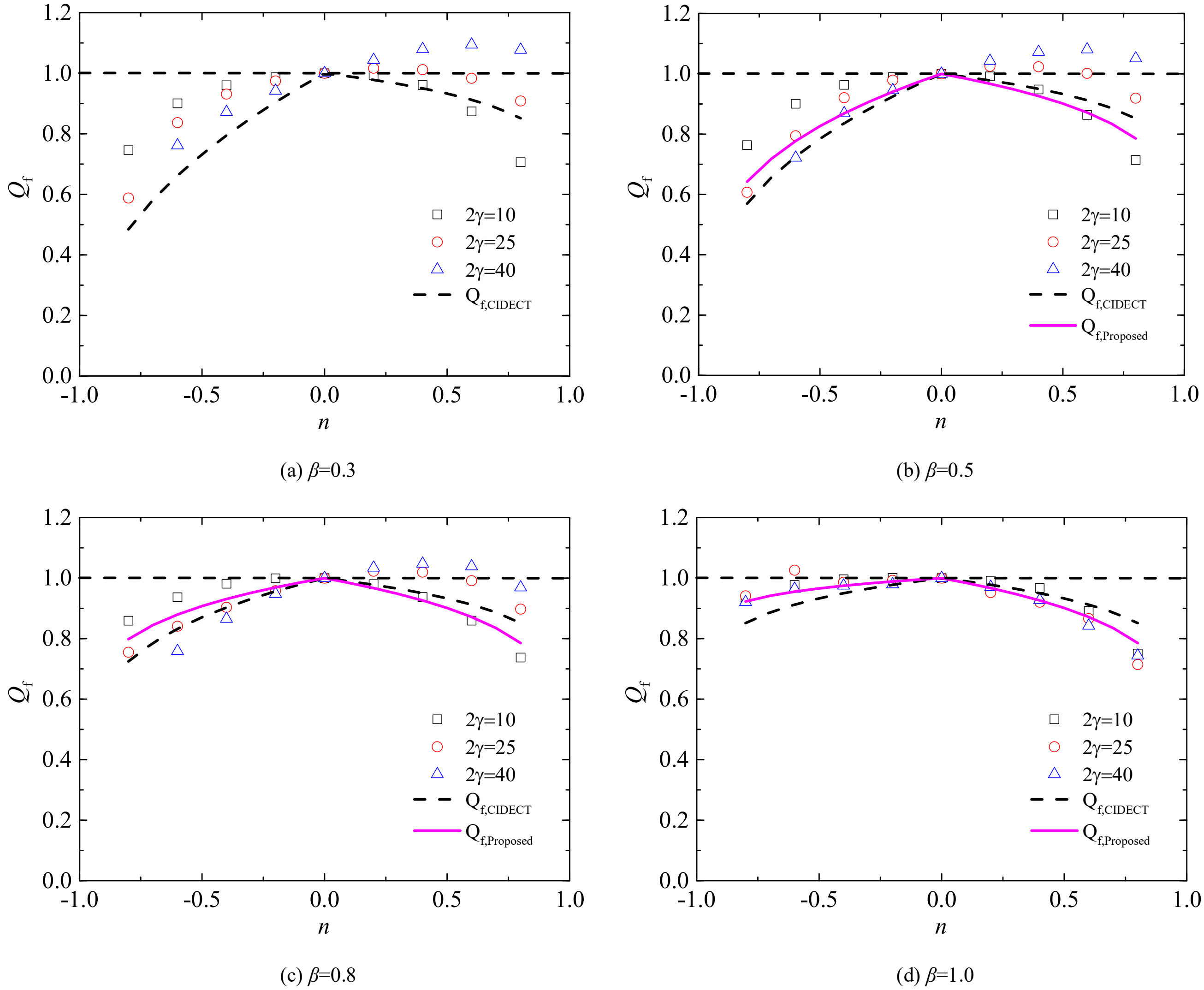

Fig. 14. Comparison of joint strength reduction for S460 RHS X-joints under chord preload.

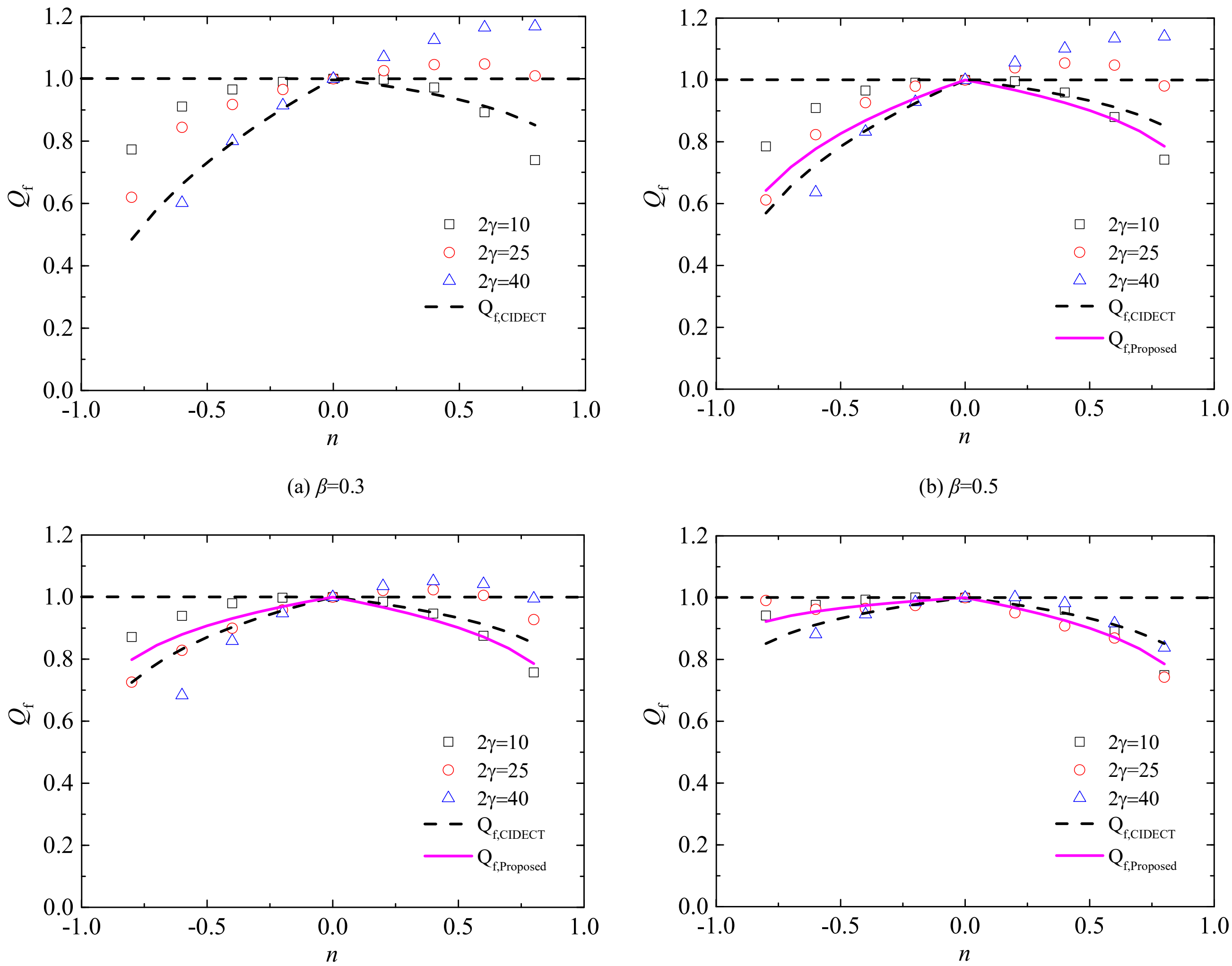

(a) β=0.3 (b) β=0.5

(c) β=0.8 (d) β=1.0

Fig. 15. Comparison of joint strength reduction for S690 RHS X-joints under chord preload.

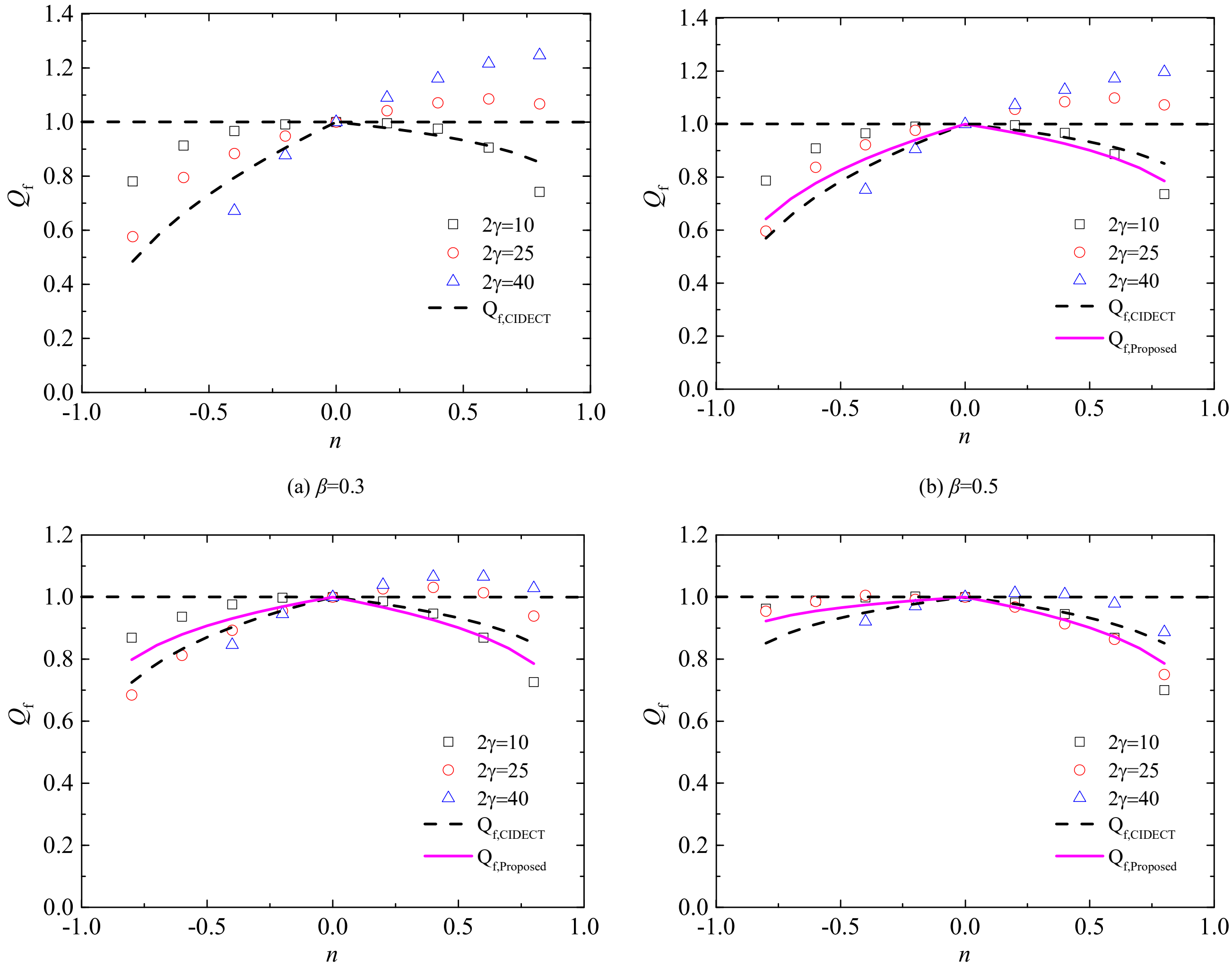

(a) β=0.3 (b) β=0.5

(c) β=0.8 (d) β=1.0

Fig. 16. Comparison of joint strength reduction for S960 RHS X-joints under chord preload.

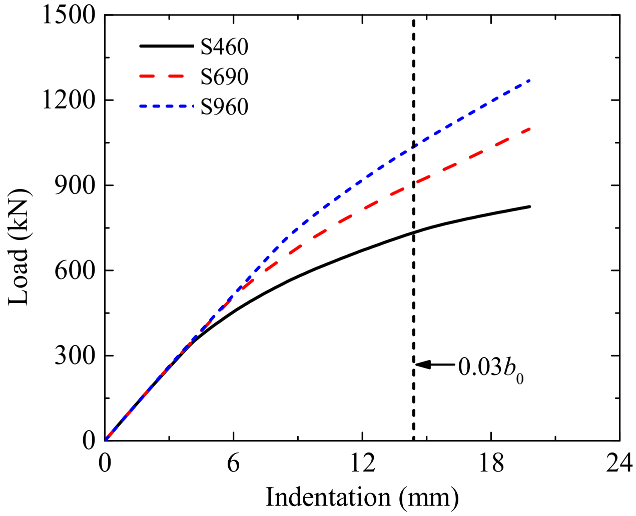

(a) β=0.3 and 2γ=25

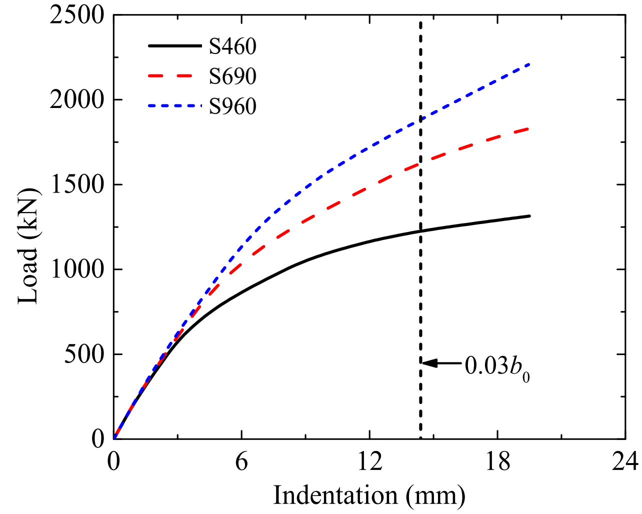

(b) β=0.5 and 2γ=25

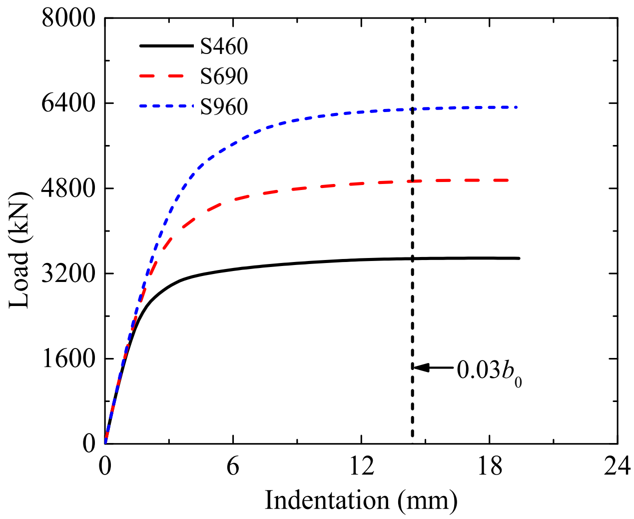

(c) β=0.8 and 2γ=25

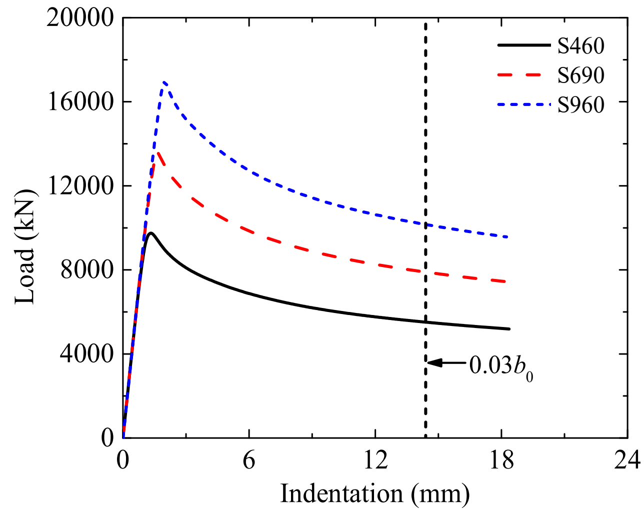

(d) β=1.0 and 2γ=25

Fig. 17. Typical load-indentation curves of fabricated RHS X-joints without chord preload.

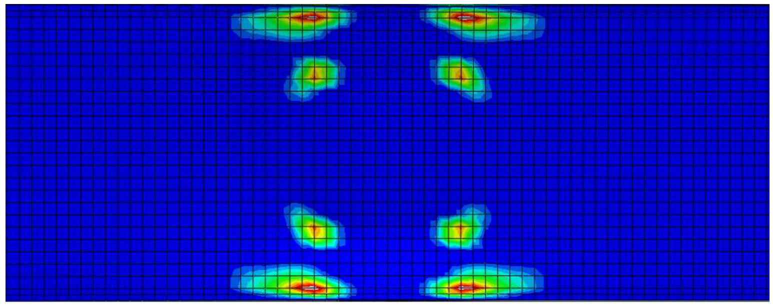

(a) S460

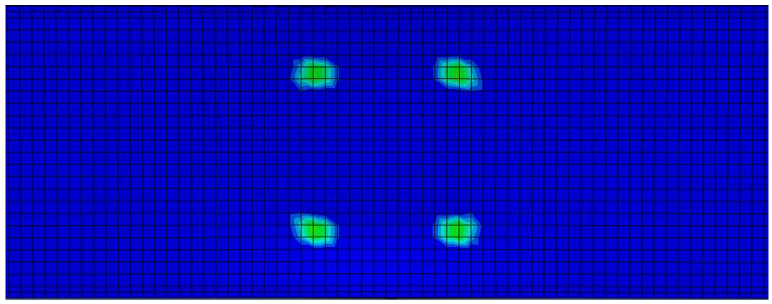

(b) S690

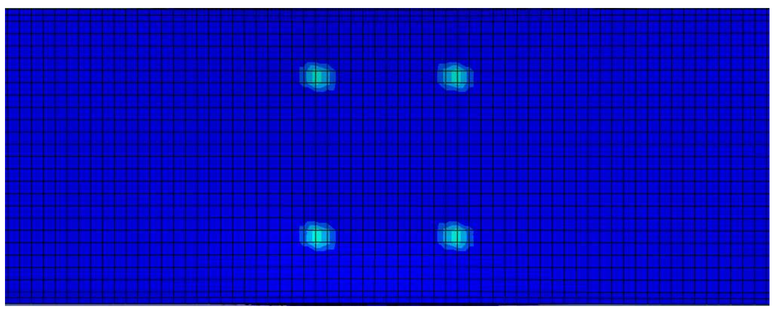

(c) S960

Fig. 18. Typical yielding patterns on chord faces of fabricated RHS X-joints with β=0.5 and 2γ=25.

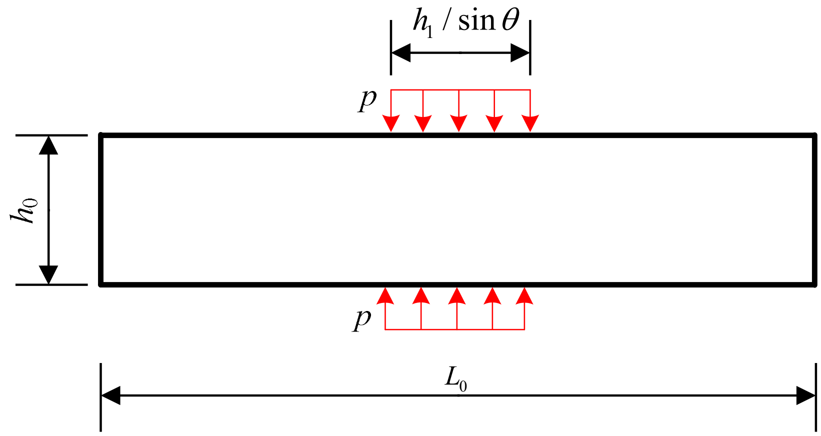

Fig. 19. Proposed analytical model for chord side wall failure in RHS X-joints.

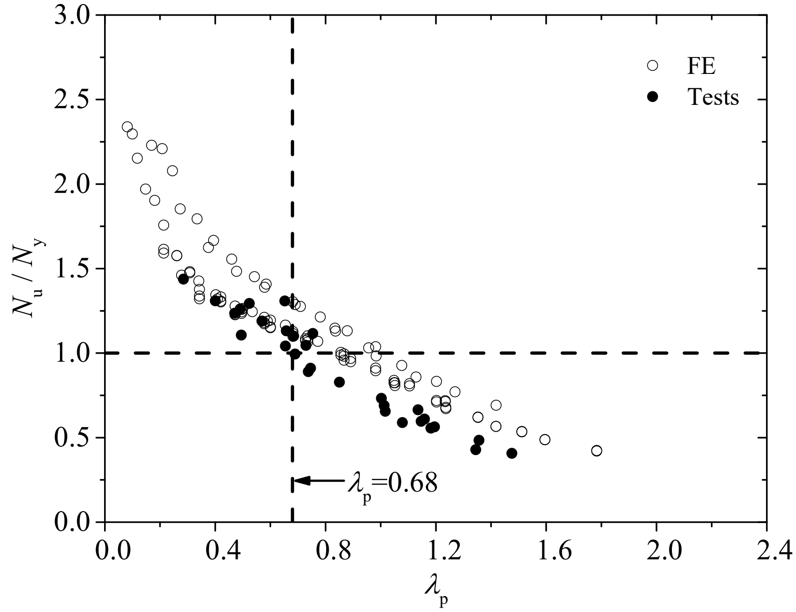

Fig. 20. Ultimate load normalised by yield load of equal-width RHS X-joints with β=1.0.

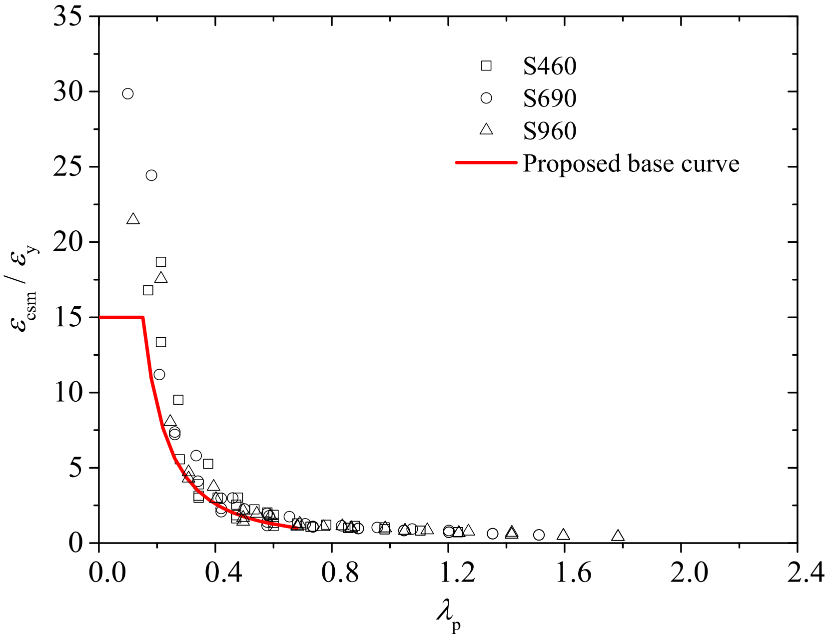

(a) Non-slender chord side walls

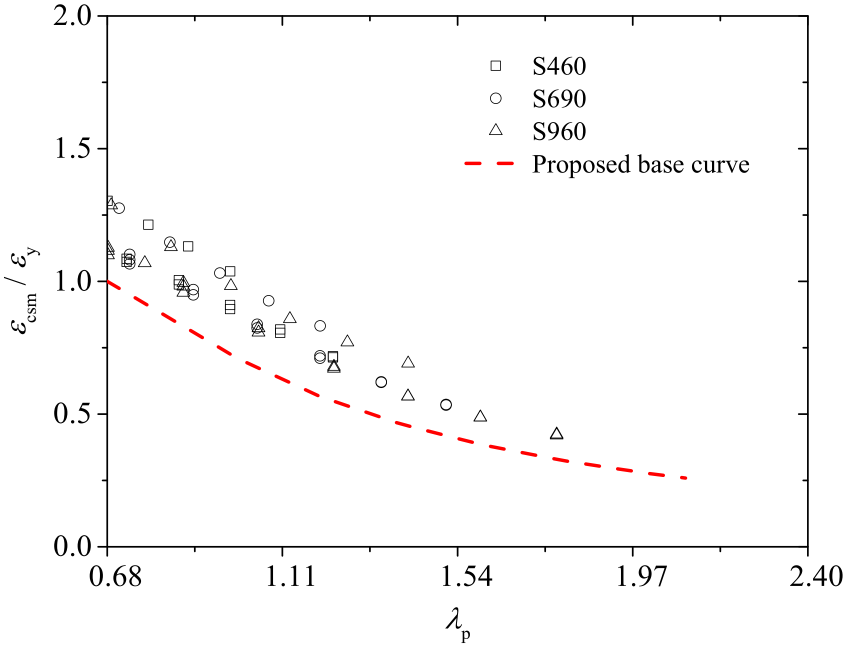

(b) Slender chord side walls

Fig. 21. Base curves for equal-width RHS X-joints with FE data.

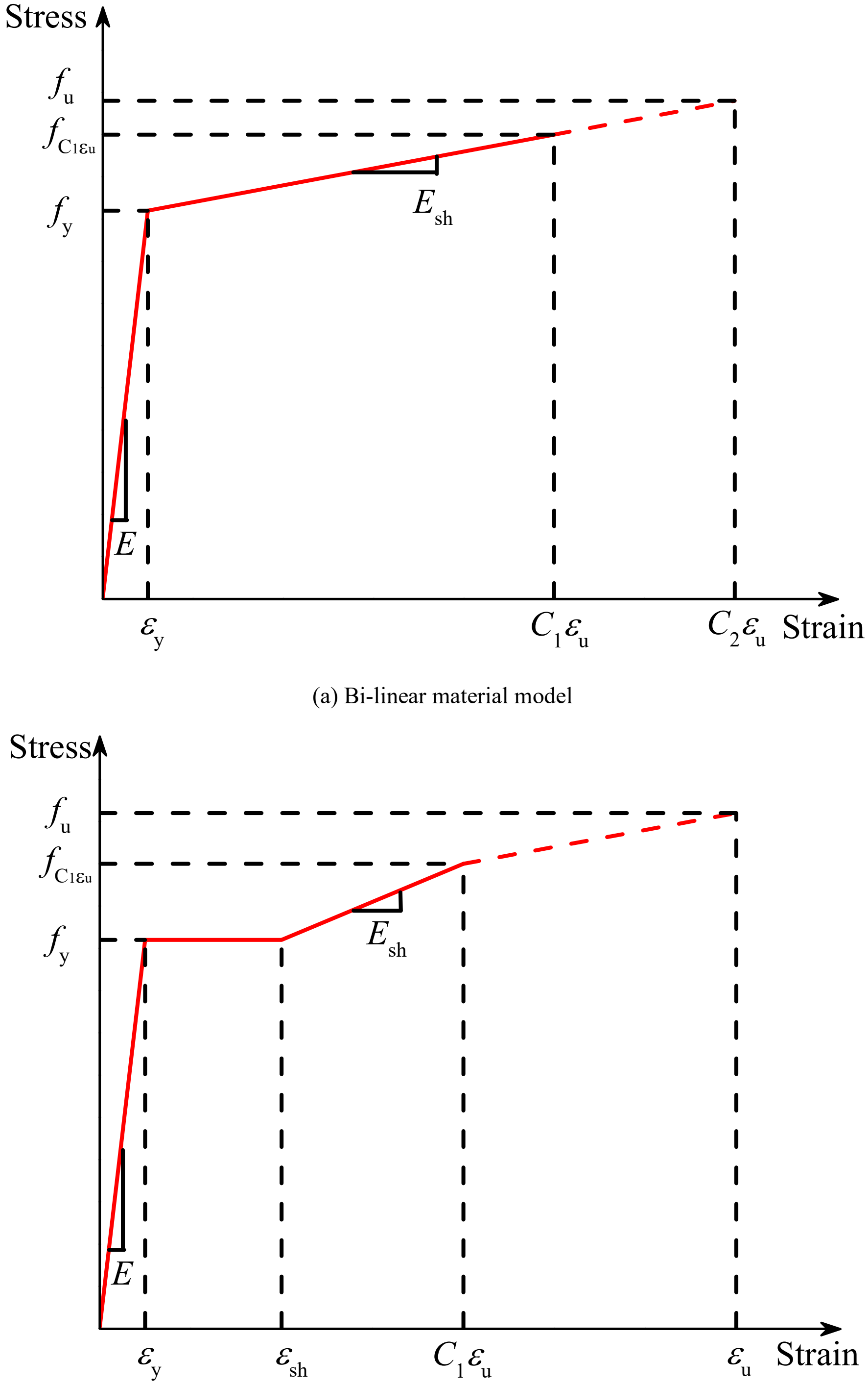

(a) Bi-linear material model

(b) Tri-linear material model

Fig. 22. CSM material models for equal-width RHS X-joints (Lan et al. [40]).

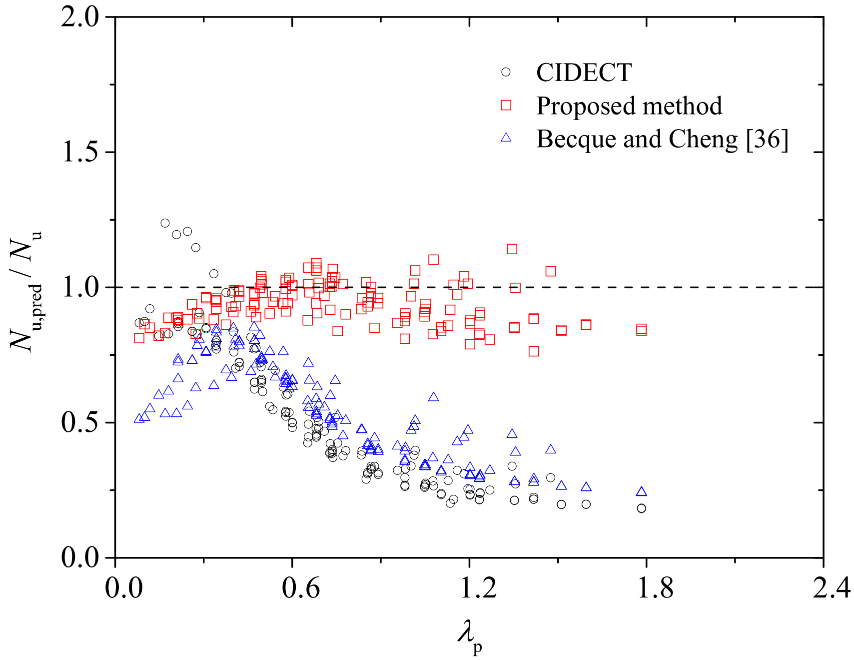

Fig. 23. Comparison of FE and test strengths of equal-width RHS X-joints with predicted strengths.

Table 1

Measured dimensions of fabricated high strength steel RHS X-joint specimens.

Specimen	b_0 (mm)	h_0 (mm)	L_0 (mm)	b_1 (mm)	h_1 (mm)	L_1 (mm)	b_w (mm)	h_w (mm)	w (mm)
X1	122.0	122.9	718	96.5	98.3	276	14.6	1.5	7.7
X1#	122.2	122.3	719	96.3	96.1	279	14.7	1.9	7.4
X2	123.0	123.1	719	80.9	81.7	233	14.3	2.0	7.8
X3	122.1	123.3	718	61.3	62.3	171	15.1	1.8	8.2
X3#	121.7	122.8	719	61.5	62.8	172	13.7	2.2	8.7
X4	181.9	182.4	1080	91.1	92.0	260	15.3	1.9	7.1
X5	240.3	242.5	1441	120.4	121.4	351	16.0	2.2	7.2
X6	301.7	301.7	1801	151.3	151.6	439	15.3	1.7	6.7

Note: # denotes repeated tests.

Table 2

Chemical compositions of high strength steel obtained from the mill certificate.

Composition	C	Si	Mn	P	S	Cr	Mo	B	Cu	CEV
Weight (%)	0.17	0.24	1.04	0.008	0.001	0.443	0.576	0.0015	0.01	0.56

Note: Carbon equivalent value, CEV = C + Mn/6 + (Cr + Mo + V)/5 + (Ni + Cu)/15.

Table 3

Measured material properties of high strength steel used in tests.

Specimen	E (GPa)	f_p (MPa)	f_y (MPa)	f_u (MPa)	ε_u (%)	ε_f (%)
F1	207.4	602.4	904.5	1012.9	5.7	15.9
F2	206.7	600.0	910.2	1019.6	4.5	15.1
Mean	207.1	601.2	907.4	1016.2	5.1	15.5

Table 4

Test results of fabricated RHS X-joint specimens.

Specimen	β	η	2γ	$3\%b_0$ (mm)	N_{Test} (kN)	N_{FE} (kN)	N_{CIDECT} (kN)	N_{FE}/N_{Test}	N_{CIDECT}/N_{Test}	$N_{Proposed}/N_{Test}$
X1	0.79	0.81	19.9	3.66	891	828	563	0.93	0.63	0.52
X1#	0.79	0.79	19.9	3.67	882	803	551	0.91	0.62	0.51
X2	0.66	0.66	20.1	3.69	541	512	366	0.95	0.68	0.56
X3	0.50	0.51	20.0	3.66	312	302	262	0.97	0.84	0.69
X3#	0.51	0.52	19.8	3.65	311	319	266	1.02	0.85	0.71
X4	0.50	0.51	29.6	5.46	256	216	264	0.84	1.03	–
X5	0.50	0.51	39.1	7.21	199	177	264	0.89	1.33	–
X6	0.50	0.50	49.1	9.05	172	161	264	0.93	1.53	–
Mean								0.93	0.94	0.60
COV								0.057	0.358	0.143

Table 5

Effects of heat affected zones on fabricated RHS X-joints in S960 steel.

FE specimen	b_0 (mm)	h_0 (mm)	t_0 (mm)	b_1 (mm)	h_1 (mm)	t_1 (mm)	β	2γ	N_{u1} (kN)	N_{u2} (kN)	N_{u2}/N_{u1}
X1	122.0	122.9	6.14	96.5	98.3	6.14	0.79	19.9	825	794	0.96
X1-1	122.0	122.9	6.14	122.0	122.9	6.14	1.00	19.9	1704	1566	0.92
X1-2	122.0	122.9	2.44	122.0	122.9	2.44	1.00	50.0	272	269	0.99
X1-3	122.0	122.9	12.20	122.0	122.9	12.20	1.00	10.0	4383	4094	0.93
X3	122.1	123.3	6.14	61.3	62.3	6.14	0.50	20.0	303	261	0.86
X3-1	122.1	123.3	6.14	24.4	24.7	6.14	0.20	20.0	105	96	0.92
X6	301.7	301.7	6.14	151.3	151.6	6.14	0.50	49.1	161	136	0.85

Note: N_{u1} and N_{u2} represent the joint strengths without and with HAZ, respectively.

Table 6

Material properties adopted for high strength steel.

Steel grade	E (GPa)	f_y (MPa)	f_u (MPa)	ε_{sh} (%)	ε_u (%)
S460	206	460	550	2.00	14.0
S690	206	690	770	0.33	8.0
S960	206	960	980	0.47	5.5
S960-R10	206	864	882	0.42	5.5
S960-R20	206	768	784	0.37	11.6

Note: The value following the letter R denotes the percentage of strength reduction compared with the base metal; ε_{sh} is the strain-hardening strain.

Table 7

Series of fabricated RHS X-joints using S460, S690 and S960 steel for the parametric study.

Series No.	b_0 (mm)	h_0 (mm)	b_1 (mm)	h_1 (mm)	β	η	ζ	2γ
1	480	480	144	144	0.3	0.3	1.0	[10-50]
2	480	480	192	192	0.4	0.4	1.0	[10-50]
3	480	480	240	240	0.5	0.5	1.0	[10-50]
4	480	480	288	288	0.6	0.6	1.0	[10-50]
5	480	480	336	336	0.7	0.7	1.0	[10-50]
6	480	480	384	384	0.8	0.8	1.0	[10-50]
7	480	480	432	432	0.9	0.9	1.0	[10-50]
8	480	480	480	480	1.0	1.0	1.0	[10-50]
9	480	480	480	240	1.0	0.5	1.0	[10-50]
10	480	240	480	240	1.0	0.5	0.5	[10-50]
11	240	480	240	480	1.0	2.0	2.0	[10-50]

Table 8

Results of statistical analysis for fabricated high strength steel RHS X-joints without chord preload.

Parameter range	N_{CIDECT}/N_{FE}			$N_{Proposed}/N_{FE}$		
	No. of data	Mean	COV	No. of data	Mean	COV
0.3≤β≤0.85	162	1.23	0.333	84	0.85	0.134
0.85<β<1.0	27	0.68	0.154	27	0.91	0.072
β=1.0	105	0.52	0.525	105	0.92	0.076
Total	294	0.93	0.522	216	0.89	0.107

Table 9

Results of statistical analysis for fabricated high strength steel RHS X-joints subjected to chord preload.

Steel grade	$Q_{f,CIDECT}/Q_{f,FE}$			$Q_{f,Proposed}/Q_{f,FE}$		
	No. of data	Mean	COV	No. of data	Mean	COV
S460	72	0.96	0.099	50	0.97	0.067
S690	72	0.94	0.099	50	0.96	0.069
S960	72	0.93	0.112	50	0.95	0.084
Total	216	0.94	0.103	150	0.96	0.074

Table 10

Fabricated RHS X-joint specimens for the elastic eigenvalue analysis.

Specimen No.	b_0 (mm)	h_0 (mm)	t_0 (mm)	b_1 (mm)	h_1 (mm)	t_1 (mm)	$f_{cr\text{-}FE}$	$f_{cr\text{-}Becque}/f_{cr\text{-}FE}$	$f_{cr\text{-}Proposed}/f_{cr\text{-}FE}$
1	480	480	48	480	240	48	16163	0.32	1.01
2	480	480	24	480	240	24	3321	0.38	1.00
3	480	480	16	480	240	16	1446	0.39	0.97
4	480	480	12	480	240	12	807	0.40	0.95
5	480	480	9.6	480	240	9.6	521	0.39	0.93
6	480	480	48	480	360	48	12124	0.28	1.03
7	480	480	24	480	360	24	2466	0.35	1.03
8	480	480	16	480	360	16	1069	0.35	1.00
9	480	480	12	480	360	12	596	0.36	0.99
10	480	480	9.6	480	360	9.6	384	0.35	0.97
11	480	480	48	480	480	48	10327	0.25	1.00
12	480	480	24	480	480	24	2001	0.32	1.05
13	480	480	16	480	480	16	865	0.33	1.02
14	480	480	12	480	480	12	482	0.33	1.01
15	480	480	9.6	480	480	9.6	311	0.33	0.99
Mean								0.34	1.00
COV								0.123	0.032

Note: All specimens with L_0=6b_0, L_1= b_1+h_1 and θ=90°.

Table 11

Comparison of strength predictions with test strengths of cold-formed and hot-finished steel RHS X-joint specimens with β=1.0.

Specimen	η	2γ	θ (°)	f_y (MPa)	N_{Test} (kN)	N_{CIDECT}/N_{Test}	N_{Becque}/N_{Test}	$N_{Proposed}/N_{Test}$
D1122 [37]	1.31	15.7	90	358	445	0.77	0.85	0.93
D1322 [37]	1.31	15.8	60	358	459	0.71	—	1.04
D2121 [37]	0.67	42.2	90	406	1315	0.52	0.63	0.90
D2122 [37]	1.49	28.3	90	406	1230	0.38	0.49	1.01
D2222 [37]	1.49	28.3	45	406	1675	0.20	—	0.92
D3121 [37]	0.76	42.1	90	392	649	0.42	0.53	0.84
D3122 [37]	1.32	31.8	90	412	530	0.40	0.51	1.06
D3221 [37]	0.76	42.1	44	392	693	0.29	—	1.02
D3222 [37]	1.32	31.8	44	412	694	0.22	—	1.01
D4132 [37]	1.00	27.2	90	406	2183	0.54	0.66	0.98
D4223 [37]	1.00	27.2	45	406	2429	0.37	—	1.07
D4323 [37]	1.00	27.2	60	406	2215	0.48	—	1.00
X1 [38]	1.00	34.4	90	330	176	0.52	0.66	1.04
X2 [38]	1.00	26.1	90	330	302	0.63	0.76	0.94
X4 [38]	1.00	17.2	90	370	560	0.84	0.85	0.91
X5 [38]	1.00	12.6	90	345	783	0.91	0.81	0.88
X6 [38]	1.00	30.0	90	463	409	0.27	0.59	1.10
X7 [38]	1.00	25.6	90	451	828	0.49	0.72	1.07
X9 [38]	1.00	37.9	90	481	1289	0.26	0.47	1.01
X-100x50x4-100x50x4 [16]	0.50	25.3	90	952	482	0.72	0.82	1.00
X-120x120x4-120x120x4 [16]	1.00	30.9	90	971	567	0.32	0.43	0.97
X-140x140x4-140x140x4 [16]	1.00	35.2	90	1008	484	0.34	0.46	1.14
X-120x120x3-120x120x3 [16]	1.00	38.7	90	1038	317	0.30	0.40	1.06
XD-C40x2-B40x2-P0 [39]	0.99	20.7	90	707	143	0.42	0.58	0.88
XD-C50x1.5-B50x1.5-P0 [39]	1.00	32.7	90	622	69.8	0.34	0.47	0.97
XD-C140x3-B140x3-P0 [39]	1.75	25.9	90	486	234	0.31	0.45	1.04
XH-C150x6-B150x6-P0 [39]	1.00	26.2	90	497	898	0.42	0.60	0.92
XH-C200x4-B200x4-P0 [39]	1.82	27.4	90	503	383	0.27	0.39	1.00
XN-C40x2-B40x2-P0 [39]	1.00	19.8	90	447	94	0.56	0.76	0.90
Mean						0.46	0.60	0.99
COV						0.417	0.253	0.075